

ARTICLE

Thioesterase PPT1 balances viral resistance and efficient T cell crosspriming in dendritic cells

Pengju Ou^{1,2}, Lifan Wen¹, Xiaoli Liu¹, Jiancheng Huang¹, Xiaoling Huang¹, Chaofei Su¹, Ling Wang¹, Hai Ni¹, Boris Reizis^{3*} , and Cliff Y. Yang^{1,4*} 

Conventional type 1 dendritic cells (cDC1s) are inherently resistant to many viruses but, paradoxically, possess fewer acidic phagosomes that enable antigen retention and cross-presentation. We report that palmitoyl-protein thioesterase 1 (PPT1), which catabolizes lipid-modified proteins in neurons, is highly expressed in cDC1s. PPT1-deficient DCs are more susceptible to vesicular stomatitis virus (VSV) infection, and mice with PPT1 deficiency in cDC1s show impaired response to VSV. Conversely, PPT1-deficient cDC1s enhance the priming of naive CD8⁺ T cells into tissue-resident KLRG1⁺ effectors and memory T cells, resulting in rapid clearance of tumors and *Listeria monocytogenes*. Mechanistically, PPT1 protects steady state DCs from viruses by promoting antigen degradation and endosomal acidification via V-ATPase recruitment. After DC activation, immediate down-regulation of PPT1 is likely to facilitate efficient cross-presentation, production of costimulatory molecules and inflammatory cytokines. Thus, PPT1 acts as a molecular rheostat that allows cDC1s to crossprime efficiently without compromising viral resistance. These results suggest potential therapeutics to enhance cDC1-dependent crosspriming.

Introduction

Antigen cross-presentation is an important pathway to prime CD8⁺ T cells in infections, cancer, and other immune-mediated pathologies (Ackerman and Cresswell, 2004; Rock and Shen, 2005). Conventional type 1 dendritic cells (cDC1s; CD8α⁺/CD103α⁺/XCR1⁺/DNGR-1⁺/BATF3-dependent DCs) are the major cross-presenting DC subset in vivo (den Haan et al., 2000; Jung et al., 2002; Hildner et al., 2008; Sancho et al., 2009; Poulin et al., 2012; Yamazaki et al., 2013; Guillemins et al., 2014; Breton et al., 2016). cDC1 development is dependent on several key transcriptional factors, such as BATF3, IRF8, ZBTB46, ID2, and ETV6 (Aliberti et al., 2003; Hacker et al., 2003; Hildner et al., 2008; Meredith et al., 2012a,b; Sichié et al., 2016; Lau et al., 2018). In addition to cDC1s, DCs derived under inflammatory conditions from hematopoietic progenitors or monocytes, and activated plasmacytoid DCs (pDCs), are also capable of cross-presentation (Helft et al., 2015; Oberkampff et al., 2018). In general, cross-presentation of exogenous antigens can occur via two major pathways. In the vacuolar pathway, antigens are directly loaded onto MHC I molecules in phagosomes. In the cytosolic pathway, antigens are exported into the cytosol and then loaded into ER or phagosomes (Joffre et al., 2012).

In cancer, cross-presentation of tumor-associated antigens is particularly crucial for an effective antitumor CD8⁺ T cell

response (Hildner et al., 2008; Fuertes et al., 2011; Roberts et al., 2016; Salmon et al., 2016; Spranger et al., 2017). In intracellular bacterial infections such as *Listeria monocytogenes* (LM), CD8⁺ T cell responses are thought to be initiated primarily by the cross-presentation of phagocytosed infected apoptotic cells (Jung et al., 2002). For certain viruses that do not directly infect DCs, crossprimed CD8⁺ T cells are essential to clear these infections (Sigal et al., 1999; Nair-Gupta and Blander, 2013). For intracellular pathogens that infect DCs, CD8⁺ T cells could also be primed by direct MHC class I presentation in infected DCs. However, it is detrimental for DCs to be infected, as intracellular infections lead to cellular damage or death, as well as manipulation of immune responses (Schwartz et al., 1996; Bowie and Unterholzner, 2008; Edelson et al., 2011). Accordingly, cDC1s had been reported to be resistant to a broad range of enveloped viruses, including HIV and the influenza virus, but their mechanism of viral resistance remains unclear (Helft et al., 2012; Silvin et al., 2017).

In comparison to macrophages, DCs maintain a higher pH in phagosomes and a lower level of lysosomal proteases (Delamarre et al., 2005). Such limited antigen degradation in DCs actually correlates with more efficient cross-presentation (Accapezzato

¹Department of Immunology, Sun Yat-sen University Zhongshan School of Medicine, Guangzhou, Guangdong, China; ²Department of Chemotherapy, First Affiliated Hospital of Fujian Medical University, Fuzhou, Fujian, China; ³Department of Pathology, New York University School of Medicine, New York, NY; ⁴Key Laboratory of Tropical Disease Control, Sun Yat-sen University, Ministry of Education, Guangzhou, Guangdong, China.

*B. Reizis and C.Y. Yang contributed equally to this paper; Correspondence to Cliff Y. Yang: yangkeli6@mail.sysu.edu.cn.

© 2019 Ou et al. This article is distributed under the terms of an Attribution–Noncommercial–Share Alike–No Mirror Sites license for the first six months after the publication date (see <http://www.rupress.org/terms/>). After six months it is available under a Creative Commons License (Attribution–Noncommercial–Share Alike 4.0 International license, as described at <https://creativecommons.org/licenses/by-nc-sa/4.0/>).

et al., 2005; Delamarre et al., 2005). DC phagosomal pH could be regulated by NADPH oxidase 2 (NOX2), which consumes the protons generated by vacuolar H⁺ adenosine triphosphatase (V-ATPase; Savina et al., 2006). In turn, NOX2 recruitment to phagosomes may be mediated by several molecules such as RAB27A, VAMP-8, RAC2, and Siglec-G (Jancic et al., 2007; Savina et al., 2009; Matheoud et al., 2013; Ding et al., 2016). Additionally, phagosomal recruitment of the ER-Golgi intermediate compartment by SEC22B may raise the pH by regulating proteasomes and lipid bodies (Bougnères et al., 2009; Cebrian et al., 2011). However, acidic phagosomes are instrumental for phagocytes to deactivate and degrade endocytosed pathogens, as many proteolytic enzymes are fully functional at a lower pH (Watts, 1997). Many viruses, including the influenza virus, rabies virus, and herpes simplex virus, are sensitive to mildly acidic pH (Stegmann et al., 1987; Roche and Gaudin, 2002; Komala Sari et al., 2013). It is unclear how cDC1s manage this apparent trade-off between efficient cross-presentation and better self-protection from viruses.

To address this question, we examined the role of palmitoyl-protein thioesterase 1 (PPT1), an enzyme that cleaves thioester-linked palmitate from S-acylated proteins in lysosomes (Camp and Hofmann, 1993). PPT1 deficiency results in infantile neuronal ceroid lipofuscinosis in humans and similar symptoms in mice (Gupta et al., 2001). Neuronal ceroid lipofuscinosis is a lysosome storage disorder (LSD) characterized by gradual neurodegeneration in the central nervous system, leading to blindness, seizures, and early death (Vesa et al., 1995). PPT1 has been previously shown to regulate synaptic vesicle recycling at nerve terminals (Kim et al., 2008). Here we demonstrated that PPT1 maintains acidic phagosomes, whereas PPT1 down-regulation after DC activation facilitates antigen retention and phagosomal acidification. Thus PPT1-deficient DCs were susceptible to viral infections but had enhanced crosspriming of naive CD8⁺ T cells into tissue-resident effector and memory cells. Our results reveal a mechanistic linkage of viral resistance and efficient cross-presentation and suggest potential therapeutic approaches to treat tumors and intracellular microbial infections.

Results

PPT1 is highly expressed in cross-presenting DCs but dispensable for their development

We first examined the specific expression of *Ppt1* mRNA by quantitative PCR (qPCR) in murine C57BL/6J WT immune cell types (Fig. 1 A). We found that *Ppt1* transcript is highly enriched in cDC1s. This result was also consistent with the cDC1-specific expression of *Ppt1* transcript in the publicly available Immunological Genome Project (IMMGEN) gene microarray and RNA sequencing (RNA-seq) databases (Fig. S1, A and B; Heng et al., 2008). We also examined CD11b⁺ MHCII⁺ CD11c⁺ DCs derived from bone marrow cells in vitro with GM-CSF/IL-4 (thereafter referred as BMDCs). *Ppt1* mRNA was expressed at a relatively high level in WT BMDCs and their GM-DC and GM-macrophage subpopulations (Fig. 1 A; Helft et al., 2015). We confirmed the PPT1 protein expression in WT cDC1s by intracellular staining,

and in WT BMDCs by Western blotting (Fig. 1, B and C). Thus, PPT1 is highly expressed on cross-presenting DCs such as cDC1s and BMDCs.

PPT1 germline knockout mice (*Ppt1*^{-/-} mice) suffer from severe neuropathology and death (commencing at ~6 mo of age; Gupta et al., 2001). Thus, to avoid the adverse effects of the neuropathology on the immune system, we generated traditional chimeras in which lethally irradiated CD45.1⁺ hosts were reconstituted from *Ppt1*^{+/+} or *Ppt1*^{-/-} bone marrow cells (hereafter referred to as *Ppt1*^{+/+} or *Ppt1*^{-/-} chimeras; Fig. S1 D). In addition, we generated two types of mixed bone marrow chimeras. First, we reconstituted lethally irradiated CD45.1.2⁺ hosts with CD45.2⁺ *Ppt1*^{-/-} bone marrow cells, mixed with equal numbers of WT CD45.1⁺ bone marrow cells (hereafter referred to as *Ppt1*^{+/+}:*Ppt1*^{-/-} chimeras; Fig. S1 E). Second, we reconstituted lethally irradiated CD45.1⁺ hosts with *Ppt1*^{+/+} or *Ppt1*^{-/-} bone marrow cells, mixed with cDC1-deficient *Batf3*^{-/-} bone marrow cells. Thus, we generated mice carrying a specific deletion of PPT1 in cDC1s (hereafter referred to as *Ppt1*^{+/+}:*Batf3*^{-/-} or *Ppt1*^{-/-}:*Batf3*^{-/-} chimeras; Fig. S1 F). We observed no defects in cDC1 percentages or cell numbers in spleen or lymph nodes in *Ppt1*^{-/-} mice or *Ppt1*^{-/-}:*Batf3*^{-/-} chimeras (Fig. S2, A-E). Since *Ppt1*^{-/-} mice engage in hyperaggressive behavior at an early age, we did not use their bone marrow cells directly for BMDCs (Gupta et al., 2001). Instead, we generated BMDCs only from *Ppt1*^{+/+} or *Ppt1*^{-/-} chimeras. BMDCs from *Ppt1*^{+/+} or *Ppt1*^{-/-} chimeras (hereafter referred to as *Ppt1*^{+/+} or *Ppt1*^{-/-} BMDCs from chimeras) were also generated at the same percentages and cell numbers (Fig. S2, F and G). All other major immune cell types appeared to be normal (Fig. S2, H and I). In addition, we cultured *Ppt1*^{+/+} or *Ppt1*^{-/-} chimera bone marrow cells with Fms-related tyrosine kinase 3 ligand (FLT3L) and OP9 stromal cells expressing the Notch ligand Delta-like 1 (OP9-DL1; Kirklind et al., 2018). These cDC1-like (DEC205⁺ CD24⁺ CD8α⁺ CD11b⁻ MHCII⁺ CD11c⁺) cells (hereafter referred as cDC1^{FL-Notch}) were also generated normally from PPT1-deficient cells (Fig. S2 J). Thus, we conclude that PPT1 is dispensable for the development of DCs.

PPT1 protects DCs and host from vesicular stomatitis virus (VSV) infection

The highly cytopathic and pantropic VSV induces a strong cytotoxic T cell response that is primed largely by cDC1s (Lichty et al., 2004; Alexandre et al., 2016). After infecting *Ppt1*^{+/+} or *Ppt1*^{-/-} BMDCs from chimeras with VSV expressing recombinant GFP (VSV-GFP) in vitro, we found that there were more than twofold more VSV-GFP⁺ *Ppt1*^{-/-} cDC1^{FL-Notch} and BMDCs from chimeras (Fig. 1 D). This difference could be due to either increased antigen uptake or an increased viral load in *Ppt1*^{-/-} DCs. To see if PPT1 regulates phagocytosis, we fed *Ppt1*^{+/+} or *Ppt1*^{-/-} BMDCs from chimeras with fluorescent plastic beads and measured the number of beads engulfed by DCs. We observed no differences in bead phagocytosis between *Ppt1*^{+/+} or *Ppt1*^{-/-} BMDCs from chimeras (Fig. S3 A). We also performed an in vivo antigen phagocytosis assay with FITC antigen spread on the skin of *Ppt1*^{+/+} or *Ppt1*^{-/-} mice and observed the intake of FITC by DCs in the skin-draining lymph nodes (Tussiwand et al., 2015). Similar to our in vitro assay, we saw no difference in FITC

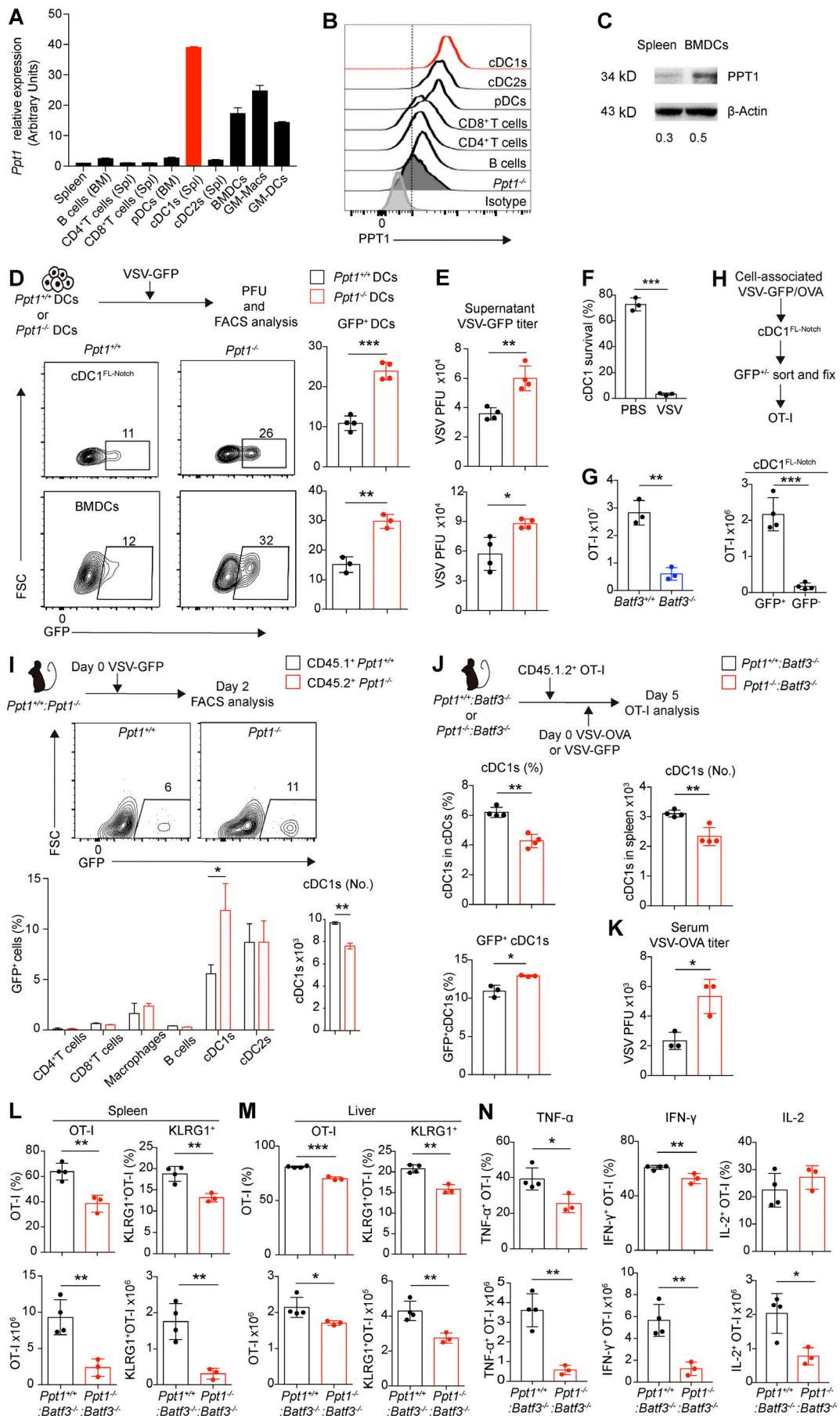


Figure 1. PPT1 protects DCs and host from VSV virus infection. (A) *Ppt1* mRNA expression. Indicated WT immune populations were FACS sorted, and *Ppt1* transcript was measured by qPCR. Data are combined results of three independent experiments ($n =$ relative values from three independent runs). (B) PPT1 protein expression in cDC1s. Indicated splenic WT immune populations were measured by intracellular FACS staining with anti-PPT1 antibodies. Data are representative of one of two independent experiments (sample from three pooled mice). (C) PPT1 protein expression in BMDCs. Indicated WT immune populations were measured by Western blotting with anti-PPT1 antibodies. β -Actin was used as loading control. Gray area ratio of PPT1 over β -actin is shown below. Data are representative of one of two independent experiments (sample from three pooled mice). (D) DC susceptibility to VSV-GFP infection in vitro. *Ppt1*^{+/+} or *Ppt1*^{-/-} cDC1^{FL-Notch} (top) or BMDCs (bottom) from chimeras were infected with VSV-GFP for 24 h and then analyzed by FACS. Representative FACS plots (left) and percentages (right) are shown. Data are representative one of three independent experiments ($n = 4$ mice per group). (E) Viral titer (PFU) of supernatant from VSV-GFP-infected cDC1^{FL-Notch} (top) or BMDCs (bottom). Data are representative of one of two independent experiments ($n = 4$ mice per group). (F) Cytopathic effect of VSV on infected cDC1s. FACS sorted WT cDC1s were incubated with VSV-GFP for 12 h, and cell survival was measured by forward scatter (FSC)/side scatter live gating. Data are representative of one of two independent experiments ($n = 3$ technical replicates). (G) OT-I response in *Batf3*^{-/-} mice. WT and *Batf3*^{-/-} mice were injected with CD45.1⁺ OT-I T cells and then infected with VSV-OVA. Splenic total OT-I cell numbers at day 6 are shown. Data are representative of one of two independent experiments ($n = 3$ mice per group). (H) Crosspriming by VSV-infected DCs. WT cDC1^{FL-Notch} were fed with cell-associated VSV-GFP/OVA and then FACS sorted based on GFP fluorescence. cDC1^{FL-Notch} were then fixed and incubated with OT-I cells for 3 d. Data are representative of one of two independent experiments ($n = 4$ technical replicates). (I) cDC1 susceptibility to VSV-GFP infection in vivo. *Ppt1*^{+/+}:*Ppt1*^{-/-} chimeras were infected with VSV-GFP. Spleen were analyzed at day 2. Representative FACS plot of cDC1s (top), GFP⁺ percentages (left), and cDC1 cell number (right) are shown. Data are representative of one of three independent experiments ($n = 3$ mice per group). (J) cDC1 susceptibility to VSV-GFP infection in vivo. *Ppt1*^{+/+}:*Batf3*^{-/-} or *Ppt1*^{-/-}:*Batf3*^{-/-} chimeras were injected with CD45.1.2⁺ OT-I T cells and the next day infected with VSV-GFP or VSV-OVA. cDC1 percentage (left) and cell numbers (center) and GFP⁺ cDC1s (right) are shown. Data are representative of one of three independent experiments ($n = 3-4$ mice per group). (K) Serum viral titer (PFU) during VSV-OVA infection. Data are representative of one of three independent experiments ($n = 3$ mice per group). (L) Splenic OT-I effector response. OT-I (l, left, gated on live CD8 α ⁺ CD44⁺ CD45.1.2⁺) and KLRG1⁺ OT-I cells (l, right), percentages (l, top), and cell numbers (l, bottom) are shown. Data are representative of one of three independent experiments ($n = 3-4$ mice per group). (M) Liver OT-I effector response. Percentages (top) and cell numbers (bottom) of OT-I (left) and KLRG1⁺ OT-I cells are shown. Data are representative of one of three independent experiments ($n = 3-4$ mice per group). (N) Cytokine production by splenic OT-I cells. Splenic cells were stimulated with SIINFEKL and analyzed by intracellular FACS staining. Percentages (top) and cell numbers (bottom) of OT-I cells that produced TNF- α (left), IFN- γ (center), and IL-2 (right) are shown. Data are representative of one of three independent experiments ($n = 3-4$ mice per group). All data are shown as mean \pm SD, and P values were calculated by two-way Student's *t* test (*, $P < 0.05$; **, $P < 0.01$; ***, $P < 0.001$).

retention in vivo in either migratory or resident cDC1s in *Ppt1*^{+/+} or *Ppt1*^{-/-} mice (Fig. S3, B and C). Next, we specifically examined active virions contained in DCs by performing a plaque-forming assay using the supernatant of infected BMDCs. We found more infectious VSV virions in the *Ppt1*^{-/-} cDC1^{FL-Notch} and BMDCs supernatant than that of *Ppt1*^{+/+} DCs from chimeras (Fig. 1 E). Our results show that PPT1-deficient DCs were more susceptible to VSV infection in vitro.

To determine if VSV is cytopathic to cDC1s, we infected WT cDC1s in vitro with VSV-GFP. We confirmed that VSV is indeed capable of lysing cDC1s efficiently (Fig. 1 F). Since *Batf3*^{-/-} mice lack cDC1s, they had a significantly diminished antiviral OT-I response (Fig. 1 G). To make sure that VSV-infected DCs are primarily responsible for the cross-presentation of cell-associated antigens, we pulsed WT cDC1^{FL-Notch} with cell-associated VSV-GFP/OVA, then sorted and fixed GFP^{+/+} DCs. After incubating DCs with OT-I cells, we found that GFP⁺ cDC1^{FL-Notch} induced a >10-fold stronger OT-I response than GFP⁻ cDC1^{FL-Notch} (Fig. 1 H). These data suggest that VSV-GFP⁺ DCs presented more cell-associated antigens and might be primarily responsible for T cell priming.

We then infected *Ppt1*^{+/+}:*Ppt1*^{-/-} chimeras with VSV-GFP and found that *Ppt1*^{-/-} cDC1s had more than twofold increased VSV-GFP⁺ staining and a reduction in total cell numbers compared with *Ppt1*^{+/+} cDC1s, while the infection rate of other lineages (cDC2s, T and B cells, and macrophages) were unaffected by PPT1 deficiency (Fig. 1 I). We also infected *Ppt1*^{+/+}:*Batf3*^{-/-} chimeras with VSV-GFP in vivo. Consistently, there were fewer surviving cDC1s are found in *Ppt1*^{-/-}:*Batf3*^{-/-} chimeras compared with *Ppt1*^{+/+}:*Batf3*^{-/-} chimeras (Fig. 1 J). Among the surviving cDC1s, more GFP⁺ cDC1s were present in *Ppt1*^{-/-}:*Batf3*^{-/-}

chimeras compared with *Ppt1*^{+/+}:*Batf3*^{-/-} chimeras (Fig. 1 J). The VSV viral titer was more than twofold higher in the serum of VSV-infected *Ppt1*^{-/-}:*Batf3*^{-/-} chimeras compared with that of *Ppt1*^{+/+}:*Batf3*^{-/-} chimeras (Fig. 1 K). Next, we examined the antigen-specific CD8⁺ T cell response in VSV-expressing recombinant ovalbumin (VSV-OVA)-infected *Ppt1*^{+/+}:*Batf3*^{-/-} or *Ppt1*^{-/-}:*Batf3*^{-/-} chimeras. We observed more than fourfold fewer OVA-specific TCR transgenic OT-I cells in the spleen (Fig. 1 L). We further examined the distribution of effector memory subsets, since killer cell lectin-like receptor family G, member 1-positive (KLRG1⁺) IL-7R α ⁻ effector CD8⁺ T cells are driven by inflammatory signals provided by DCs (Joshi et al., 2007). There were more than threefold fewer KLRG1⁺ IL-7R α ⁻ effector OT-I cells in *Ppt1*^{-/-}:*Batf3*^{-/-} compared with *Ppt1*^{+/+}:*Batf3*^{-/-} chimeras (Fig. 1 L). We also observed a similar reduction of OT-I cells and KLRG1⁺ IL-7R α ⁻ effector in the liver (Fig. 1 M). IFN- γ - and TNF- α -producing OT-I CD8⁺ T cells decreased by at least fourfold in *Ppt1*^{-/-}:*Batf3*^{-/-} chimeras compared with *Ppt1*^{+/+}:*Batf3*^{-/-} chimeras (Fig. 1 N). Thus, we found that *Ppt1*^{-/-}:*Batf3*^{-/-} chimeras had diminished CD8⁺ T cell response to VSV infection compared with *Ppt1*^{+/+}:*Batf3*^{-/-} chimeras, likely due to increased infection rates and reduced survival of PPT1-deficient cDC1s.

PPT1-deficient cDC1s enhance antitumor immune response

Unlike VSV, cancerous cells pose no immediate existential threat to cDC1s. cDC1s not only crossprime tumor-specific CD8⁺ T cells, but also enhance checkpoint-blockade efficacy (Salmon et al., 2016). We used two tumor transplantation models, MC38 colorectal and B16F10 melanoma cancer, to examine the effect of PPT1 deficiency in cDC1s during the antitumor immune response. After transplanting *Ppt1*^{-/-}:*Batf3*^{-/-} and *Ppt1*^{+/+}:*Batf3*^{-/-}

chimeras with MC38 or B16F10 stably transfected with recombinant OVA (B16-OVA), we observed more than two-fold smaller MC38 and B16-OVA tumors in *Ppt1^{-/-}:Batf3^{-/-}* chimeras than those of *Ppt1^{+/+}:Batf3^{-/-}* chimeras at day 35 (Fig. 2, A and B). Consistent with previous reports, *Batf3^{-/-}* mice, which lack crosspriming cDC1s, had >2 fold larger MC38 tumors than *Ppt1^{+/+}:Batf3^{-/-}* chimeras at day 35 (Hildner et al., 2008; Fig. 2 A). The lower B16-OVA tumor burden in *Ppt1^{-/-}:Batf3^{-/-}* chimeras resulted in a higher survival rate compared with *Ppt1^{+/+}:Batf3^{-/-}* chimeras (Fig. 2 C). Next, we adoptively transferred equal numbers of *Ppt1^{+/+}* or *Ppt1^{-/-}* BMDCs from chimeras into WT mice transplanted with B16-OVA, and mice that received *Ppt1^{-/-}* BMDCs from chimeras had a higher survival rate than mice that received *Ppt1^{+/+}* BMDCs from chimeras (Fig. 2 D). Thus, we conclude that PPT1 deficiency in cDC1s inhibits tumor growth.

We then examined the endogenous antigen-specific tumor-infiltrating CD8⁺ T cells in the solid tumors of the chimeras. We found approximately twofold more CD103⁺ SIINFEKL-H2-K^b tetramer⁺ CD8⁺ T cells residing in the tumors at day 25 (Fig. 2 E). Next, we sought to examine the trafficking pattern of cross-primed CD8⁺ T cells by injecting naive OT-I CD8⁺ T cells into mice bearing the B16-OVA xenograft. After 3 d, we observed more than fivefold more intratumor CD44⁺ OT-I cells in *Ppt1^{-/-}:Batf3^{-/-}* chimeras compared with *Ppt1^{+/+}:Batf3^{-/-}* chimeras (Fig. 2 F). Tumor-infiltrating OT-I effectors from *Ppt1^{-/-}:Batf3^{-/-}* chimeras expressed more than sixfold less PD-1 compared with those in *Ppt1^{+/+}:Batf3^{-/-}* chimeras (Fig. 2 G). We also observed a more than fourfold increase in IFN- γ production by OT-I cells from tumor-draining lymph nodes in *Ppt1^{-/-}:Batf3^{-/-}* chimeras compared with *Ppt1^{+/+}:Batf3^{-/-}* chimeras (Fig. 2 H). These results suggest that tumor-resident effector and memory CD8⁺ T cell responses are enhanced in *Ppt1^{-/-}:Batf3^{-/-}* chimeras.

Exhausted T cells and formation of tissue-resident memory (T_{RM}) cells in lymphocytic choriomeningitis virus clone 13 (LCMV CLI3) infections are well characterized and are proposed to be similar to the antitumor T cell response (Wherry and Kurachi, 2015; Amsen et al., 2018). While capable of infecting DCs, LCMV CLI3 is noncytopathic and suppresses DC immune functions (Ng et al., 2011). After infecting the chimeras with LCMV CLI3, we saw less lung tissue damage and infiltrated lymphocytes in *Ppt1^{-/-}:Batf3^{-/-}* chimeras compared with *Ppt1^{+/+}:Batf3^{-/-}* chimeras (Fig. 2 I). Accordingly, we observed an approximately threefold lower viral titer in *Ppt1^{-/-}:Batf3^{-/-}* chimeras compared with *Ppt1^{+/+}:Batf3^{-/-}* chimeras measured by LCMV-mRNA-specific qPCR in the kidney (Fig. 2 J). There were also more intraepithelial CD69⁺ CD103⁺ LCMV H2-D^b GP33 tetramer⁺ CD8⁺ T cells in the *Ppt1^{-/-}:Batf3^{-/-}* chimeras compared with *Ppt1^{+/+}:Batf3^{-/-}* chimeras (Fig. 2 K). These results suggest that antiviral resident memory CD8⁺ T cell responses are enhanced in *Ppt1^{-/-}:Batf3^{-/-}* chimeras.

PPT1-deficient cDC1s convey host with resistance to LM

Intracellular bacteria LM do not kill DCs directly, but specifically use live cDC1s as an efficient vehicle to disseminate (Edelson et al., 2011). At the same time, LM clearance is heavily dependent on CD8⁺ T cells cross-primed by cDC1s (Jung et al., 2002; Alexandre et al., 2016). After infecting the chimeras with LM

expressing recombinant OVA (LM-OVA), we observed a massive decrease in LM bacterial burden, as measured by CFUs, in the liver (>450-fold) and spleen (>40-fold) of *Ppt1^{-/-}:Batf3^{-/-}* chimeras compared with *Ppt1^{+/+}:Batf3^{-/-}* chimeras (Fig. 3 A). The bacterial load in *Ppt1^{-/-}:Batf3^{-/-}* chimeras was comparable to that of *Batf3^{-/-}* mice, which are largely resistant to LM due to the lack of cDC1s (Fig. 3 A; Edelson et al., 2011). To eliminate the possibility that PPT1 might affect the survival of LM-infected cDC1s, we examined splenic cDC1s during LM-OVA infection in vivo. We observed no difference in cDC1 percentages or cell numbers between infected *Ppt1^{+/+}:Batf3^{-/-}* or *Ppt1^{-/-}:Batf3^{-/-}* chimeras at day 5 (Fig. 3 B). We also measured LM CFU from lysates of sorted *Ppt1^{+/+}* or *Ppt1^{-/-}* cDC1s from infected *Ppt1^{-/-}:Batf3^{-/-}* and *Ppt1^{+/+}:Batf3^{-/-}* chimeras. We found that PPT1-deficient cDC1s were infected at the same rate as PPT1-sufficient cDC1s (Fig. 3 C). Here we demonstrate that mice with PPT1 deficiency in cDC1s are resistant to LM infection.

Next, we assessed whether the LM resistance in PPT1-deficient chimeras was dependent on CD8⁺ T cells primed by DCs. To determine whether CD8⁺ T cells primed by PPT1-deficient cDC1s were more cytotoxic, we used an in vivo killing assay using high expression of carboxyfluorescein diacetate succinimidyl ester (CFSE^{hi}; empty control) or CFSE^{int} (loaded with SIINFEKL) WT splenocytes (Iborra et al., 2012). We found that more SIINFEKL-pulsed target cells were lysed by effector CD8⁺ T cells from *Ppt1^{-/-}:Batf3^{-/-}* chimeras (Fig. 3 D). To exclude the possibility that NK1.1⁺ cells played a role in the killing assay, we found that NK1.1⁺ DX5⁺ cell numbers appeared to be normal and that they produced similar amounts of IFN- γ in infected chimeras (Fig. S4, A and B). The production of IL-12p40 also remained unchanged in the serum of LM-OVA infected *Ppt1^{+/+}:Batf3^{-/-}* or *Ppt1^{-/-}:Batf3^{-/-}* chimeras (Fig. S4 C). Next, we adoptively transferred equal numbers of *Ppt1^{+/+}* or *Ppt1^{-/-}* BMDCs from chimeras into LM-OVA-infected WT mice, and we observed a >1,000-fold lower bacterial load in liver of WT mice that received *Ppt1^{-/-}* BMDCs than mice with *Ppt1^{+/+}* BMDCs from chimeras (Fig. 3 E). IFN- γ and TNF- α production by OT-I cells were also increased by >2-fold in mice that received *Ppt1^{-/-}* BMDCs from chimeras (Fig. 3 E). Hexadecylsulfonylfluoride (HDSF) is a small molecule inhibitor of PPT1 enzymatic activity (Das et al., 2000). Since direct injection of HDSF into mice is lethal, we used an adoptive transfer system in which BMDCs were treated with HDSF ex vivo (Fig. S4 D). Similarly, we found >300-fold reduction of liver bacterial burden in the infected WT mice that received HDSF-treated BMDCs, compared with the mice that received DMSO-treated BMDCs (Fig. 3 F). IFN- γ and TNF- α production by OT-I cells were also increased in mice that received HDSF-treated BMDCs (Fig. 3 F). Thus, we conclude that the rapid clearance of LM in PPT1-deficient mice is due to enhanced CD8⁺ T cell priming by PPT1-deficient DCs.

PPT1-deficient cDC1s preferentially crossprime naive CD8⁺ T cells into KLRG1⁺ effectors at nonlymphoid tissue

Having observed enhanced crosspriming by PPT1-deficient cDC1s to tumors and LM, we sought to directly test the cross-priming abilities of cDC1s in vivo. Hence, we intravenously injected CFSE-labeled OT-I cells and cell-associated OVA into

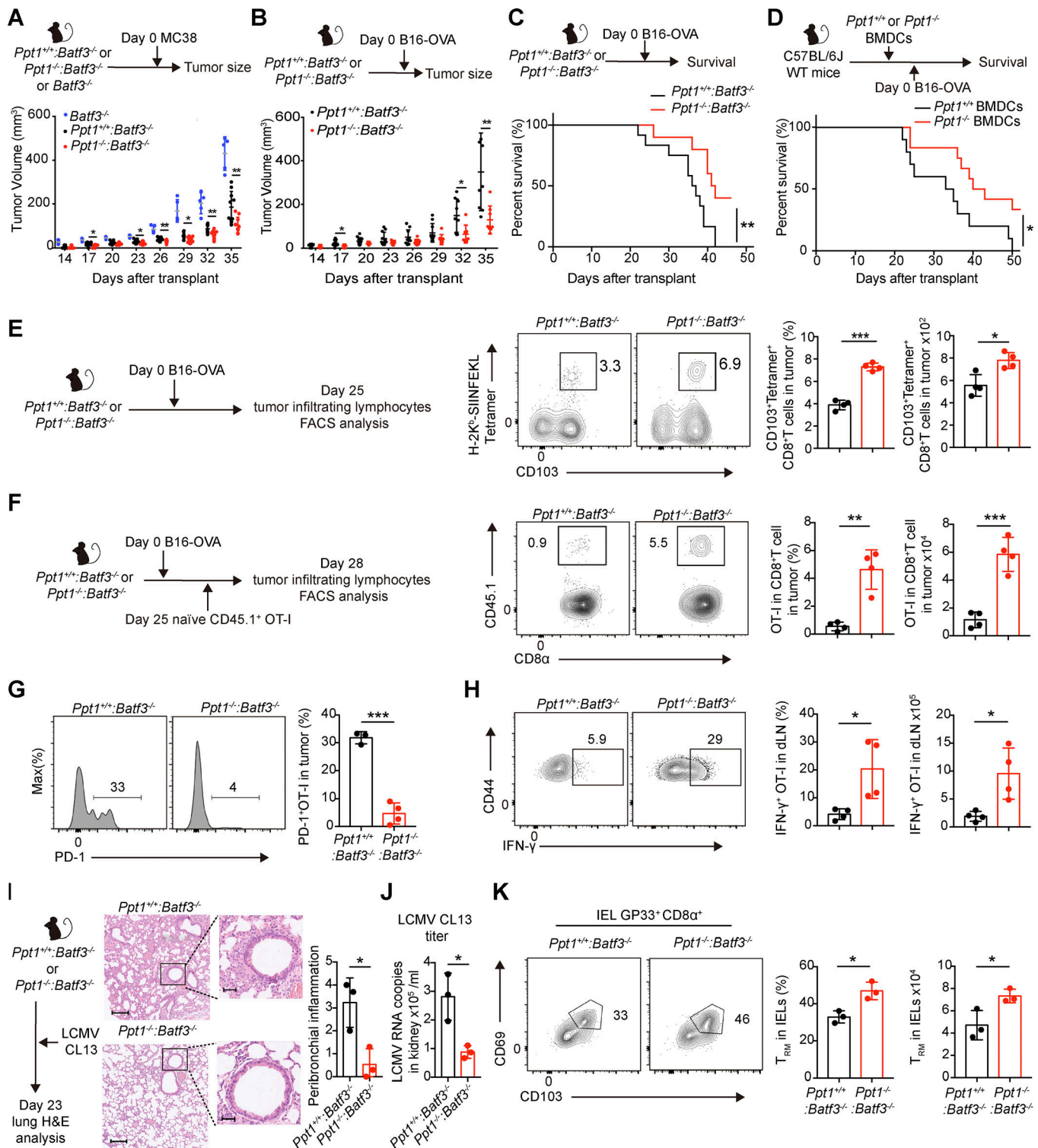


Figure 2. PPT1-deficient cDC1s enhance antitumor immune response. (A) MC38 tumor growth curve. *Batf3*^{-/-} mice, *Ppt1*^{+/+}:*Batf3*^{-/-}, or *Ppt1*^{-/-}:*Batf3*^{-/-} chimeras were transplanted with MC38. Data are representative of one of three independent experiments (*Batf3*^{-/-}, *n* = 5 mice; *Ppt1*^{+/+}:*Batf3*^{-/-} or *Ppt1*^{-/-}:*Batf3*^{-/-}, *n* = 10 mice). (B) B16-OVA tumor growth curve. *Ppt1*^{+/+}:*Batf3*^{-/-} or *Ppt1*^{-/-}:*Batf3*^{-/-} chimeras were transplanted with B16-OVA. Data are representative of one of three independent experiments (*Ppt1*^{+/+}:*Batf3*^{-/-}, *n* = 12 mice; *Ppt1*^{-/-}:*Batf3*^{-/-}, *n* = 9 mice). (C) B16-OVA survival curve of chimeras. *Ppt1*^{+/+}:*Batf3*^{-/-} or *Ppt1*^{-/-}:*Batf3*^{-/-} chimeras were transplanted with B16-OVA. Data are representative of one of three independent experiments (*Ppt1*^{+/+}:*Batf3*^{-/-}, *n* = 12 mice; *Ppt1*^{-/-}:*Batf3*^{-/-}, *n* = 9 mice). (D) B16-OVA survival curve of WT mice receiving BMDCs from chimeras. WT mice received *Ppt1*^{+/+} or *Ppt1*^{-/-} BMDCs from chimeras, and then were transplanted with B16-OVA. Data are representative of one of three independent experiments (*Ppt1*^{+/+}, *n* = 10 mice; *Ppt1*^{-/-}, *n* = 12 mice). (E) Tumor-infiltrating antigen-specific CD8⁺ T cells. *Ppt1*^{+/+}:*Batf3*^{-/-} or *Ppt1*^{-/-}:*Batf3*^{-/-} chimeras were transplanted with B16-OVA, and tumor-infiltrating lymphocytes (gated on live CD8α⁺ CD44⁺ B220⁻ cells) from solid tumors were analyzed at day 25 by FACS. Percentages (left) and cell numbers (right) are shown. Data are representative of one of two independent experiments (*n* = 4 mice per group). (F) Tumor-infiltrating OT-I cells. Tumor-infiltrating lymphocytes

(gated on live CD8 α^+ CD44 $^+$ cells) were analyzed by FACS in solid tumors from *Ppt1* $^{+/+}$:*Batf3* $^{-/-}$ or *Ppt1* $^{-/-}$:*Batf3* $^{-/-}$ chimeras with B16-OVA xenograft. Percentages (left) and cell numbers (right) are shown. Data are representative of one of two independent experiments ($n = 4$ mice per group). (G) PD-1 expression on tumor-infiltrating OT-I cells. OT-I cells (gated on live CD8 α^+ CD44 $^+$ CD45.1.2 $^+$ cells) were analyzed in solid tumors from *Ppt1* $^{+/+}$:*Batf3* $^{-/-}$ or *Ppt1* $^{-/-}$:*Batf3* $^{-/-}$ chimeras with B16-OVA xenograft. Histogram (left) and MFI (right) are shown. Data are representative of one of two independent experiments ($n = 4$ mice per group). (H) IFN- γ production of OT-I cells in tumor-draining lymph node (dLN). Tumor-draining lymph node cells (gated on live CD8 α^+ CD44 $^+$ cells) from *Ppt1* $^{+/+}$:*Batf3* $^{-/-}$ or *Ppt1* $^{-/-}$:*Batf3* $^{-/-}$ chimeras with B16-OVA xenograft were stimulated with SIINFEKL. Representative FACS plot (left), percentages (center), and cell numbers (right) are shown. Data are representative of one of two independent experiments ($n = 4$ mice per group). (I) Representative H&E lung section (left) and semiquantitative score of peribronchial inflammation (right). *Ppt1* $^{-/-}$:*Batf3* $^{-/-}$ chimeras were infected with LCMV CL 13 and analyzed at day 23. Bars, 200 μ m (left) or 50 μ m (right). Data are representative of one of two independent experiments ($n = 3$ mice per group). (J) Viral load in kidney. LCMV CL 13 viral mRNA in kidney tissue extracts were measured by qPCR. Data are combined results of three independent experiments ($n =$ relative values from three independent runs). (K) Intraepithelial antigen-specific resident memory T cells. Intraepithelial lymphocytes (gated on live CD8 α^+ CD44 $^+$ GP33 $^+$ B220 $^-$ cells) were analyzed by FACS. Representative FACS plot (left), percentages (center), and cell numbers (right) are shown. Data are representative of one of two independent experiments ($n = 3$ mice per group). All data are shown as mean \pm SD, and P values were calculated by two-way Student's t test (*, $P < 0.05$; **, $P < 0.01$; ***, $P < 0.001$). IEL, intraepithelial lymphocyte.

Ppt1 $^{+/+}$:*Batf3* $^{-/-}$ or *Ppt1* $^{-/-}$:*Batf3* $^{-/-}$ chimeras (Moore et al., 1988; den Haan et al., 2000). We observed more than threefold more OT-I cells (in both percentages and cell numbers) in *Ppt1* $^{-/-}$:*Batf3* $^{-/-}$ chimeras compared with *Ppt1* $^{+/+}$:*Batf3* $^{-/-}$ chimeras in the liver and blood (Fig. 4, A and B). In comparison, there was no difference in splenic OT-I cell percentages or numbers (Fig. 4, A and B). We further examined the distribution of the KLRG1 $^+$ IL-7R α^- effector subset, since they are more cytotoxic and tend to localize in nonlymphoid tissue (Joshi et al., 2007). We found that KLRG1 $^+$ IL-7R α^- effector CD8 $^+$ T cells formed more readily in the liver and spleen (more than fourfold based on percentages, more than threefold based on cell numbers) of *Ppt1* $^{-/-}$:*Batf3* $^{-/-}$ chimeras compared with *Ppt1* $^{+/+}$:*Batf3* $^{-/-}$ chimeras (Fig. 4, C–E).

During LM infection, cross-presentation of phagocytosed infected apoptotic cells by cDCs initiates the CD8 $^+$ T cell response (Jung et al., 2002). We observed a similar pattern of CD8 $^+$ T cell trafficking and subset formation in LM-OVA-infected *Ppt1* $^{+/+}$:*Batf3* $^{-/-}$ or *Ppt1* $^{-/-}$:*Batf3* $^{-/-}$ chimeras. A greater number of expanded OT-I cells was observed in the liver and blood, but not the spleen, in *Ppt1* $^{-/-}$:*Batf3* $^{-/-}$ chimeras compared with *Ppt1* $^{+/+}$:*Batf3* $^{-/-}$ chimeras (Fig. 4, F and G). We also found more KLRG1 $^+$ IL-7R α^- effector CD8 $^+$ T cells in liver, blood, and spleen (Fig. 4, H and I). At later time points, there was no difference in the total number of KLRG1 $^+$ IL-7R α^+ or KLRG1 $^+$ IL-7R α^- effector CD8 $^+$ T cells in blood in LM-OVA-infected chimeras (Fig. S5, A–C). We observed no difference in central memory or effector memory subsets in blood, liver, and spleen OT-I cells at day 7 (Fig. S5, D–F). Collectively, our data suggest that PPT1-deficient cDCs preferentially cross-prime naive CD8 $^+$ T cells into KLRG1 $^+$ IL-7R α^- effectors at nonlymphoid tissue.

PPT1 promotes antigen degradation and phagosomal acidification in DCs

To explain the opposing phenotypes caused by PPT1 deficiency in cDCs, we examined the role of PPT1 in the antigen presentation pathway of DCs. To determine whether PPT1 regulates antigen degradation in DCs, we performed a phagosomal protein degradation assay with OVA-associated beads using *Ppt1* $^{+/+}$ or *Ppt1* $^{-/-}$ cDC1 $^{FL-Notch}$ and BMDCs from chimeras. We found approximately twofold less degraded OVA protein in phagosomes of *Ppt1* $^{-/-}$ than *Ppt1* $^{+/+}$ cDC1 $^{FL-Notch}$ and BMDCs from chimeras during the time course (Fig. 5 A). Additionally, we fed DQ-OVA, which produces fluorescence upon

hydrolysis by proteases, to the *Ppt1* $^{+/+}$ or *Ppt1* $^{-/-}$ cDC1 $^{FL-Notch}$ and BMDCs from chimeras, and we detected reduced DQ signals in *Ppt1* $^{-/-}$ than *Ppt1* $^{+/+}$ cDC1 $^{FL-Notch}$ and BMDCs from chimeras (Fig. 5 B). Then, we treated WT BMDCs with DMSO or HDSF and measured antigen degradation using OVA-associated beads or DQ-OVA. Consistently, we found that HDSF-treated WT BMDCs degraded approximately twofold less OVA and released less DQ fluorescence than DMSO-treated BMDCs (Fig. 5, A and B). Therefore, we conclude that PPT1 promotes antigen degradation in DCs.

Since antigen uptake differentially impacts antigen presentation by DCs, we already determined that PPT1 does not affect the phagocytosis ability of DCs (Fig. S3; Kamphorst et al., 2010). Then, we examined whether the slower antigen degradation in PPT1-deficient DCs is due to a more acidic endosomal pH. We measured the phagosomal pH of *Ppt1* $^{+/+}$ or *Ppt1* $^{-/-}$ cDC1 $^{FL-Notch}$ and BMDCs from chimeras with pH-sensitive fluorescent pHrodo-OVA beads along with pH-insensitive AF488 beads. We found that the phagosomal pH was approximately 1 log higher in *Ppt1* $^{-/-}$ than *Ppt1* $^{+/+}$ cDC1 $^{FL-Notch}$ and BMDCs from chimeras (Fig. 5 C). We also found that HDSF-treated WT BMDCs had almost half a log higher phagosomal pH than DMSO-treated BMDCs (Fig. 5 C). These results suggest that PPT1 promotes phagosomal acidification in DCs.

Phagocytes use acidic phagosomes to deactivate and degrade engulfed infectious agents (Watts, 1997). To assess whether VSV loses infectivity under acidic treatment, we treated VSV-OVA virions with different acidic pH conditions for as little as 30 min and found that VSV-OVA lost infectivity as the pH decreased (Fig. 5 D). In contrast to VSV, treatment of LM-OVA with different acidic pH conditions did not affect its infectivity (Fig. 5 E). We triggered endosomal alkalization in WT cDC1 $^{FL-Notch}$ with low concentrations of NH $_4$ Cl and found that this treatment is sufficient to trigger an increase in VSV-GFP infection (Fig. 5 F; Jancic et al., 2007). Our data suggest that PPT1-mediated acidic phagosomes protect DCs from VSV infection.

The classic pH regulator V-ATPase, which consumes ATP to pump protons from the cytosol, had been shown to be crucial for maintaining the DC phagosomal pH (Cebrian et al., 2011). To further dissect the relationship between V-ATPase and PPT1, we purified DC phagosomes and found PPT1-deficient DC phagosomes had lower levels of V-ATPase subunit V1 $_a$ (Fig. 5 G). We also used confocal microscopy to observe the localization of

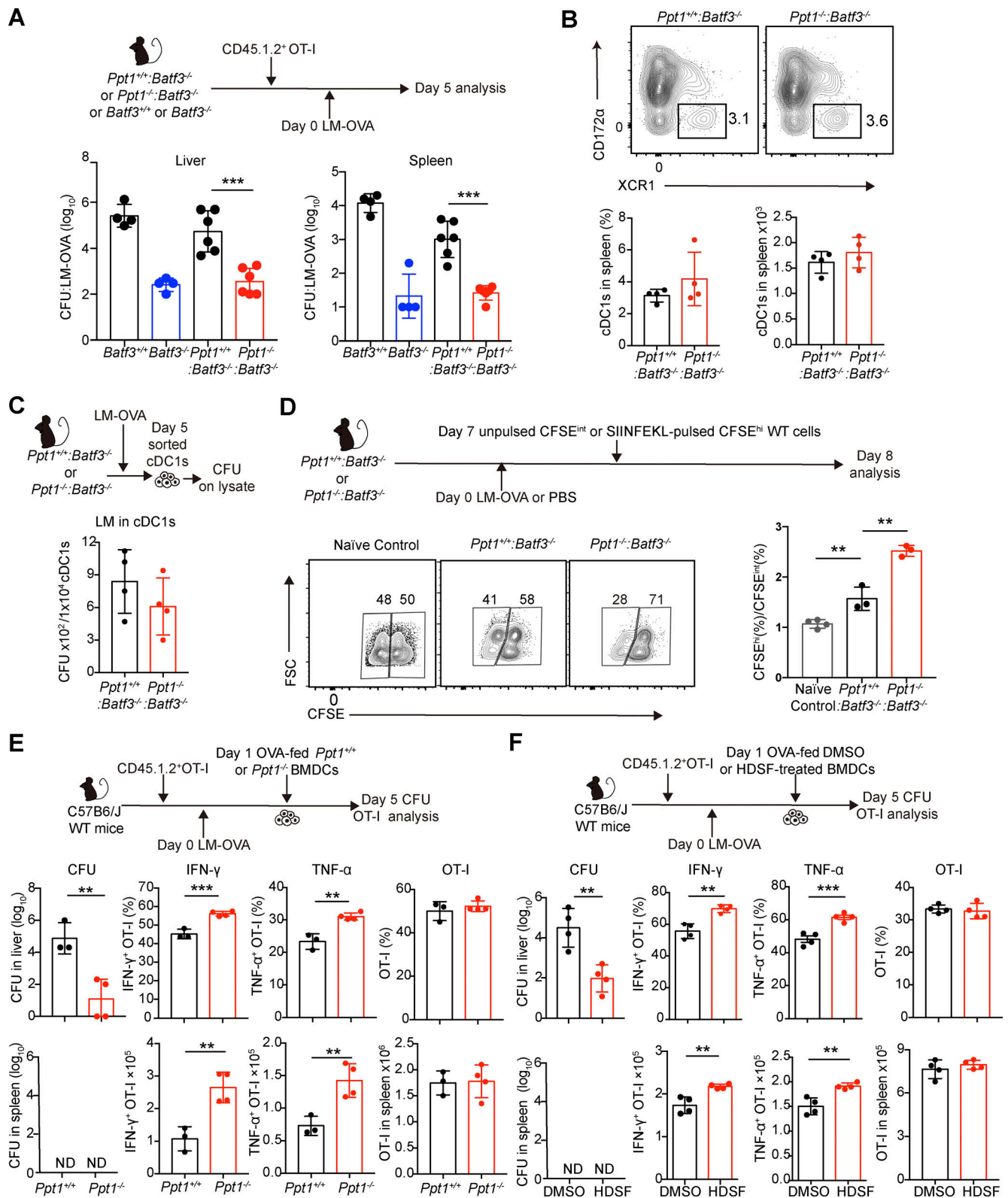


Figure 3. PPT1-deficient cDC1s convey host with resistance to LM. (A) Bacterial load (CFU) of liver (left) and spleen (right) are shown. *Batf3*^{+/+} or *Batf3*^{-/-} mice or *Ppt1*^{+/+}:*Batf3*^{-/-} or *Ppt1*^{-/-}:*Batf3*^{-/-} chimeras were injected with CD45.1.2⁺ OT-I T cells and the next day infected with LM-OVA. Mice were analyzed at day 5. Data are representative of one of five independent experiments (*Batf3*^{+/+}, *n* = 4 mice; *Batf3*^{-/-}, *n* = 4 mice; *Ppt1*^{+/+}:*Batf3*^{-/-} or *Ppt1*^{-/-}:*Batf3*^{-/-}, *n* = 6 mice). (B) Survival of splenic cDC1s. Representative FACS plot (left, gated on live MHCII⁺ CD11c⁺ CD172α⁺ XCR1⁺), percentages (center), and cell numbers (right) are shown. Data are representative of one of two independent experiments (*n* = 4 mice per group). (C) Bacterial burden in cDC1s. cDC1s (gated on live MHCII⁺ CD11c⁺ CD172α⁺ XCR1⁺ cells) from *Ppt1*^{+/+}:*Batf3*^{-/-} or *Ppt1*^{-/-}:*Batf3*^{-/-} chimeras were FACS sorted at day 5, and their lysates were used for CFU plating. Data are representative of one of two independent experiments (*n* = 4 mice per group). (D) Cytotoxicity of antigen-specific CD8⁺ T cells in vivo. LM-OVA-infected

chimeras were injected with SIINFEKL-pulsed/CFSE-labeled WT cells. Representative FACS plot (left) and CFSE^{hi}/CFSE^{int} ratio (right) are shown. Data are representative of one of two independent experiments ($n = 3$ mice per group). **(E and F)** Bacterial load (CFU) and cytokine production by OT-I cells in WT mice receiving BMDCs. LM-OVA-infected WT mice received either *Ppt1*^{+/+} or *Ppt1*^{-/-} BMDCs from chimeras (E) or DMSO or HDSF-treated WT BMDCs (F). Liver and spleen samples were plated for CFU, and splenic OT-I cells (gated on live CD8 α ⁺ CD44⁺ CD45.1.2⁺ cells) were stimulated with SIINFEKL and analyzed by intracellular staining. Data are representative of one of three independent experiments ($n = 4$ mice per group). All data are shown as mean \pm SD, and P values were calculated by two-way Student's *t* test (**, $P < 0.01$; ***, $P < 0.001$). FSC, forward scatter.

V-ATPase subunit V1_a in *Ppt1*^{+/+} or *Ppt1*^{-/-} BMDCs from chimeras, and we found that V-ATPase colocalized less with LAMP1⁺ vesicles in *Ppt1*^{-/-} DCs than in *Ppt1*^{+/+} DCs (Fig. 5 H). We then performed an in vitro cross-presentation assay with OVA-associated beads, along with Concanamycin B (conB), an inhibitor of V-ATPase (Jancic et al., 2007). The difference in OT-I proliferation between *Ppt1*^{+/+} and *Ppt1*^{-/-} BMDCs disappeared after conB treatment (Fig. 5 I). Thus, we demonstrate that PPT1 lowers endosomal pH by recruiting V-ATPase to DC phagosomes.

PPT1 suppresses antigen cross-presentation in vivo and in vitro

Higher cross-presentation capacity is associated with slower antigen degradation and higher phagosomal pH (Accapezzato et al., 2005; Delamarre et al., 2005). When we performed the in vivo cross-presentation assay with cell-associated OVA, we found that splenic OT-I cells from *Ppt1*^{-/-}:*Batf3*^{-/-} chimeras expanded much faster compared with those from *Ppt1*^{+/+}:*Batf3*^{-/-} chimeras (Fig. 6 A). We also observed approximately twofold increased production of IFN- γ by splenic OT-I CD8⁺ T cells in terms of percentages and cell numbers in *Ppt1*^{-/-}:*Batf3*^{-/-} chimeras compared with *Ppt1*^{+/+}:*Batf3*^{-/-} chimeras (Fig. 6, B–D). In contrast, TNF- α and IL-2 production by OT-I cells remained unchanged (Fig. 6, C and D). We noticed a greater activation of the crossprimed CD8⁺ T cells, as CD44 was up-regulated and CD8 α was down-regulated in OT-I cells from *Ppt1*^{-/-}:*Batf3*^{-/-} chimeras that those from *Ppt1*^{+/+}:*Batf3*^{-/-} chimeras (Fig. 6 E). Our data suggest that PPT1 in cDC1s suppresses the proliferation and IFN- γ production of crossprimed CD8⁺ T cells in vivo.

Next, we performed in vitro cross-presentation assays with exogenous antigens and measured the proliferation of OT-I cells by Cell Proliferation Dye. Consistent with our in vivo data, we found that PPT1-deficient cDC1^{FL-Notch} crossprimed more OT-I cells when pulsed with various concentrations of OVA (Fig. 6 F). Similar to cDC1^{FL-Notch}, we observed increased OT-I proliferation by cell-associated OVA, soluble OVA, and OVA-associated beads in *Ppt1*^{-/-} BMDCs from chimeras (Fig. 6 G). OT-I cells crossprimed by *Ppt1*^{-/-} BMDCs from chimeras produced higher levels of IFN- γ than *Ppt1*^{+/+} BMDCs from chimeras (Fig. 6 H). We also found that treating WT BMDCs in vitro with HDSF greatly enhanced the crosspriming ability of BMDCs, with more rapid proliferation and increased IFN- γ production in OT-I cells (Fig. 6, I–K). Here we find that PPT1 in DCs suppresses proliferation and IFN- γ production of crossprimed CD8⁺ T cells in vitro.

To determine if PPT1 regulates the endogenous MHC I presentation pathway, we measured and observed no difference in MHC class I (H2-K^b) expression between *Ppt1*^{+/+} or *Ppt1*^{-/-} cDC1s in steady state, after in vivo LM-OVA infection or ex vivo LPS

activation (Fig. 6 L). Furthermore, we transduced *Ppt1*^{+/+} or *Ppt1*^{-/-} BMDCs from chimeras with an OVA-overexpressing retrovirus, and detected no difference in endogenous presented MHC class I antigen (measured by anti-H-2K^b-SIINFEKL complex antibody 25.D1.16) and OT-I proliferation (Fig. 6 M). Lastly, to exclude the possibility that if PPT1-deficient DCs could prime CD8⁺ T cells independently of cross-presented antigens, we pulsed *Ppt1*^{+/+} or *Ppt1*^{-/-} cDC1^{FL-Notch} with various concentration of SIINFEKL and found that there was no difference in OT-I proliferation (Fig. 6 N). Here we conclude that PPT1 is dispensable for the endogenous MHC I presentation pathway in DCs.

Rapid down-regulation of PPT1 in activated cDC1s facilitates efficient crosspriming

DC cross-presentation capacity is usually increased after activation by TLRs (Alloatti et al., 2015). To elucidate the regulation of PPT1 during DC activation, we examined the expression of *Ppt1* mRNA transcripts in activated DCs by qPCR. We observed that *Ppt1* mRNA was significantly down-regulated in polyinosinic:polycytidylic acid (poly(I:C))-treated cDC1s (>100-fold) and LPS-treated BMDCs (>20-fold) following in vitro stimulation for 16 h (Fig. 7, A and B). When we reanalyzed a previously published RNA-seq that profiled immune cells during murine cytomegalovirus infection in vivo, we also found that PPT1 mRNA was down-regulated in cDC1s (Fig. S1 C; Manh et al., 2013). After this acute down-regulation, we then observed an up-regulation of *Ppt1* mRNA in cDC1s and BMDCs 48 h after stimulation (Fig. 7, A and B). In contrast, cDC2s and pDCs had relatively low transcript amounts of *Ppt1* before and after activation (Fig. 7 C). Next, we confirmed the PPT1 protein expression pattern in LPS-activated BMDCs by Western blotting (Fig. 7 D). Here, we find that PPT1 expression is quite dynamic in cross-presenting DCs: high expression at steady state, low expression after TLR activation, and recovery at a later time point.

To dissect the kinetic relationship between PPT1 down-regulation and efficient cross-presentation, we further examined the expression of PPT1 mRNA by qPCR at 0.5, 1, 3, and 5 h after activation by poly(I:C) or LPS in WT BMDCs, and we found a gradual decrease of PPT1 mRNA expression starting 0.5~1 h after activation (Fig. 7, E and F). We also found a corresponding increase in phagosomal pH in WT BMDCs 0.5~1 h after LPS activation (Fig. 7 G). Thus, we found that PPT1 down-regulation and endosomal acidification happen concurrently, as early as 0.5~1 h after activation. Furthermore, we fed OVA to BMDCs transduced with PPT1-overexpressing retroviruses, then found that CD8⁺ T cell crosspriming is decreased compared with BMDCs transduced with empty viruses (Fig. 7 H). Our results show that down-regulation of PPT1 may be responsible for enhanced cross-presentation in activated DCs.

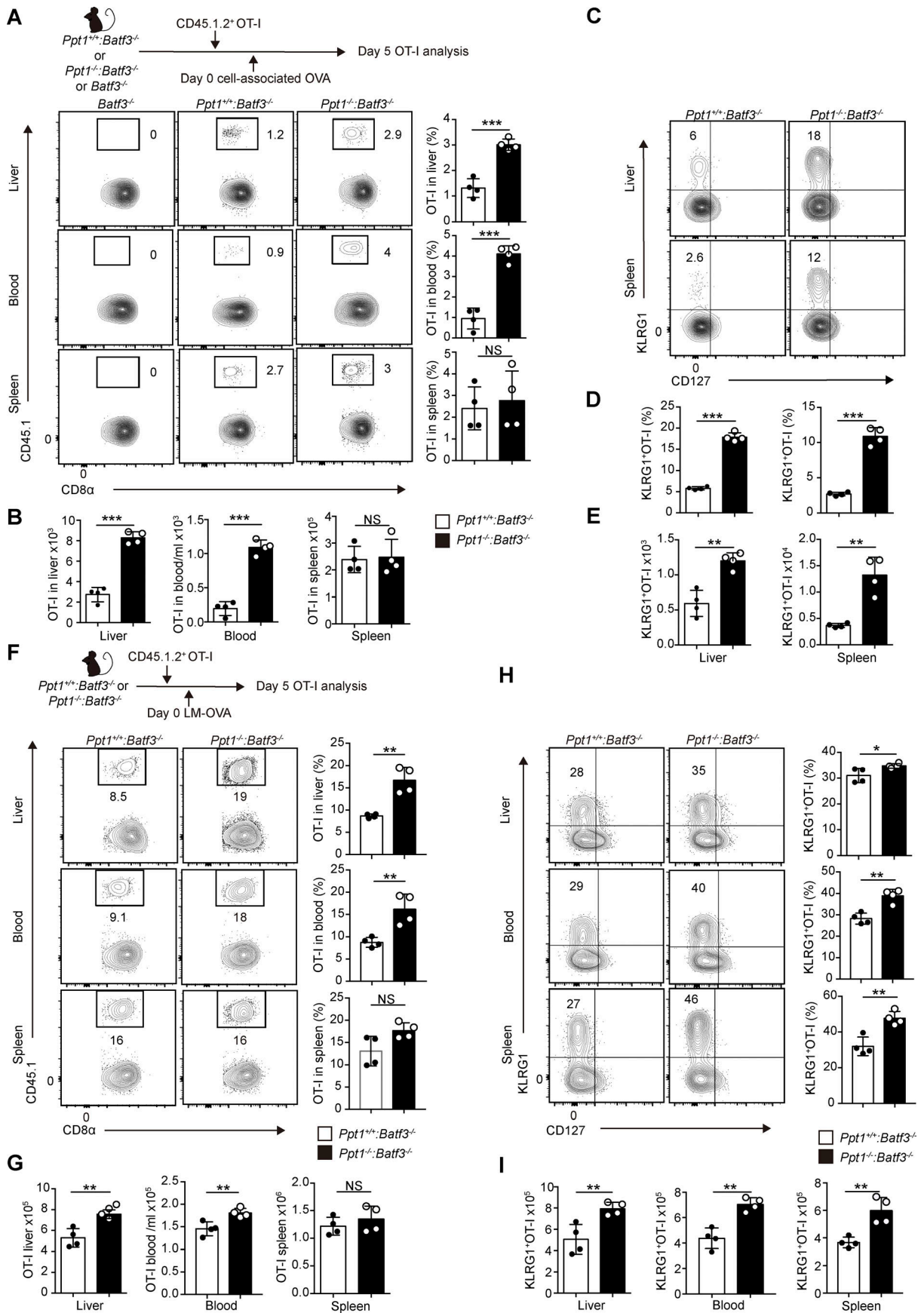


Figure 4. PPT1-deficient cDC1s preferentially crossprime naive CD8⁺ T cells into KLRG1⁺ effectors at nonlymphoid tissue. (A and B) Tissue distribution of crossprimed OT-I cells. CD8⁺ T cells (gated on live CD8 α^+ CD44 $^+$) were analyzed from indicated organs from *Ppt1*^{+/+}:*Batf3*^{-/-} or *Ppt1*^{-/-}:*Batf3*^{-/-} chimeras. Representative FACS plots (A, left) of liver (top), blood (center), and spleen (bottom); percentages (A, right); and cell numbers (B) are shown. Data are representative of one of five independent experiments ($n = 4$ mice per group). **(C-E)** Distribution of crossprimed OT-I effector subsets. OT-I cells (gated on live CD8 α^+ CD44 $^+$ CD45.1.2 $^+$ cells) were analyzed from *Ppt1*^{+/+}:*Batf3*^{-/-} or *Ppt1*^{-/-}:*Batf3*^{-/-} chimeras in indicated organs. Representative FACS plot (C) of liver (top) and spleen (bottom), percentages (D), and cell numbers (E) are shown. Data are representative of one of five independent experiments ($n = 4$ mice per group). **(F and G)** Tissue distribution of OT-I cells during infection. Representative FACS plots (F, left) of liver (top), blood (center), and spleen (bottom); percentages (F, right); and cell numbers (G) are shown. Data are representative of one of five independent experiments ($n = 4$ mice per group). **(H and I)** Distribution of OT-I effector subsets during infection. OT-I (gated on live CD8 α^+ CD44 $^+$ CD45.1.2 $^+$ cells) effector subsets from *Ppt1*^{+/+}:*Batf3*^{-/-} or *Ppt1*^{-/-}:*Batf3*^{-/-} chimeras were analyzed in the indicated organs. Representative FACS plots (H, left) of liver (top), blood (center), and spleen (bottom); percentages (H, right); and cell numbers (I) are shown. Data are representative of one of five independent experiments ($n = 4$ mice per group). All data are shown as mean \pm SD, and P values were calculated by two-way Student's *t* test (*, $P < 0.05$; **, $P < 0.01$; ***, $P < 0.001$).

Since the stimulatory signals provided by DCs influence effector and memory T cell differentiation, we hypothesized that the artificial deletion of PPT1 might control T cell priming signals (Kaeche and Cui, 2012). We detected increased expression of CD86, CD80, and CD40 in PPT1-deficient cDC1s from in vivo LM-OVA infection (Fig. 7 I). PPT1-deficient cDC1s activated by LPS ex vivo produced increased expression of CD86 compared with PPT1-sufficient cDC1s (Fig. 7 J). *Ppt1*^{-/-} BMDCs from chimeras activated by LPS in vitro expressed increased levels of CD80, CD86, and CD40 compared with *Ppt1*^{+/+} BMDCs (Fig. 7 K). However, we did not observe any difference in CD24 expression in *Ppt1*^{+/+} or *Ppt1*^{-/-} cDC1s during in vivo LM-OVA infection or ex vivo LPS activation (Fig. 7, J and K). Our data suggest that deletion of PPT1 in activated DCs facilitates expression of costimulatory molecules.

The production of cytokines, such as IL-12, has been proposed to facilitate cDC1 crosspriming of naive cells into memory T cell subsets (Mashayekhi et al., 2011; Sosinowski et al., 2013; Kim et al., 2014). Accordingly, we found that activated *Ppt1*^{-/-} cDC1s produced more IL-12p40 and TNF- α than *Ppt1*^{+/+} cDC1s upon poly(I:C) or LPS activation (Fig. 7 L). We also found increased production of IL-12p40 and TNF- α by *Ppt1*^{-/-} BMDCs from chimeras (Fig. 7 M). Since cDC1-derived IL-12 is crucial for host protection against *Toxoplasma gondii*, we infected the chimeras with *T. gondii* and measured the amount of IL-12p40 in the serum by ELISA (Mashayekhi et al., 2011). We observed a consistently higher serum level of IL-12p40 in *Ppt1*^{-/-}:*Batf3*^{-/-} chimeras than in *Ppt1*^{+/+}:*Batf3*^{-/-} chimeras throughout the time course (Fig. 7 N). Here we conclude that the deletion of PPT1 in activated DCs leads to increased production of inflammatory cytokines. Collectively, our results suggest that the down-regulation of PPT1 in activated DCs is likely to facilitate naive T cell priming by increased cross-presentation and production of costimulatory and inflammatory cytokines.

Discussion

We demonstrated that PPT1 deficiency in cDC1s is detrimental to the host in cytopathic viral infections but beneficial when encountering tumors and intracellular bacteria. We hypothesize that high levels of PPT1 in steady-state cDC1s maintain protective acidic phagosomes to deactivate viruses, whereas low levels of PPT1 in activated cDC1s are likely to facilitate T cell cross-priming with increased stimulatory signals. Despite PPT1 being

down-regulated after activation, we still observed that complete loss of PPT1 in activated cDC1s increases the expression of costimulatory B7 molecules and inflammatory cytokines such as IL-12. Thus, PPT1-deficient cDC1s lacked this “on-off switch” and remained in a constant state of enhanced cross-presentation.

Our data suggest that PPT1 in DCs promotes phagosome acidification for increased viral resistance. First, we showed that PPT1-deficient DCs had more alkaline phagosomes. This could be due to reduced recruitment of V-ATPases, which directly lowers pH by pumping in protons. Our results are consistent with a recent study showing that PPT1 regulates lysosomal pH and V-ATPase recruitment in neurons (Bagh et al., 2017). Second, we demonstrated that VSV infectivity was lowered by a brief duration of mild acidic treatment. Similarly, preexposure of herpes simplex virus to mildly acidic pH inactivates viral infectivity in an irreversible manner (Weed et al., 2017). Correspondingly, we found that endosomal alkalization in DCs also increased their VSV infection rate. Third, we found that PPT1-deficient DCs were more easily infected by VSV in vitro and in vivo, and PPT1-deficient DCs released more virions into the surroundings. Thus, the impaired response to VSV by PPT1-deficient cDC1s may be due to a failure to deactivate phagocytosed virions in DC phagosomes. Of note, the weakened anti-VSV T cell response in PPT1-deficient mice might be partially rescued by increased crosspriming by PPT1-deficient cDC1s. In comparison, LCMV CL13 is noncytopathic, and increased LCMV infection of PPT1-deficient DCs may not affect cDC1 survival as much as VSV. The negative impact of increased LCMV infection may then be easily countered by the enhanced cDC1 priming of tissue-resident T cells. To confirm that the viral resistance conferred by PPT1 is mediated by acidic phagosomes, more cytopathic and noncytopathic viruses should be examined.

The upstream regulation of PPT1 in DCs remains to be fully elucidated. Many groups have observed that DCs could switch to different “modes” of cross-presentation capability (Joffre et al., 2012). DCs usually enhance cross-presentation upon activation by TLRs or cytokines such as IFN-I, but then decrease it after returning to the steady state (Fuertes et al., 2011; Mantegazza et al., 2014; Alloatti et al., 2015; Samie and Cresswell, 2015). Since we found that PPT1 inhibits cross-presentation, DCs are likely to down-regulate PPT1 quickly after TLR ligation to facilitate efficient cross-presentation. Thus, further experiments are needed

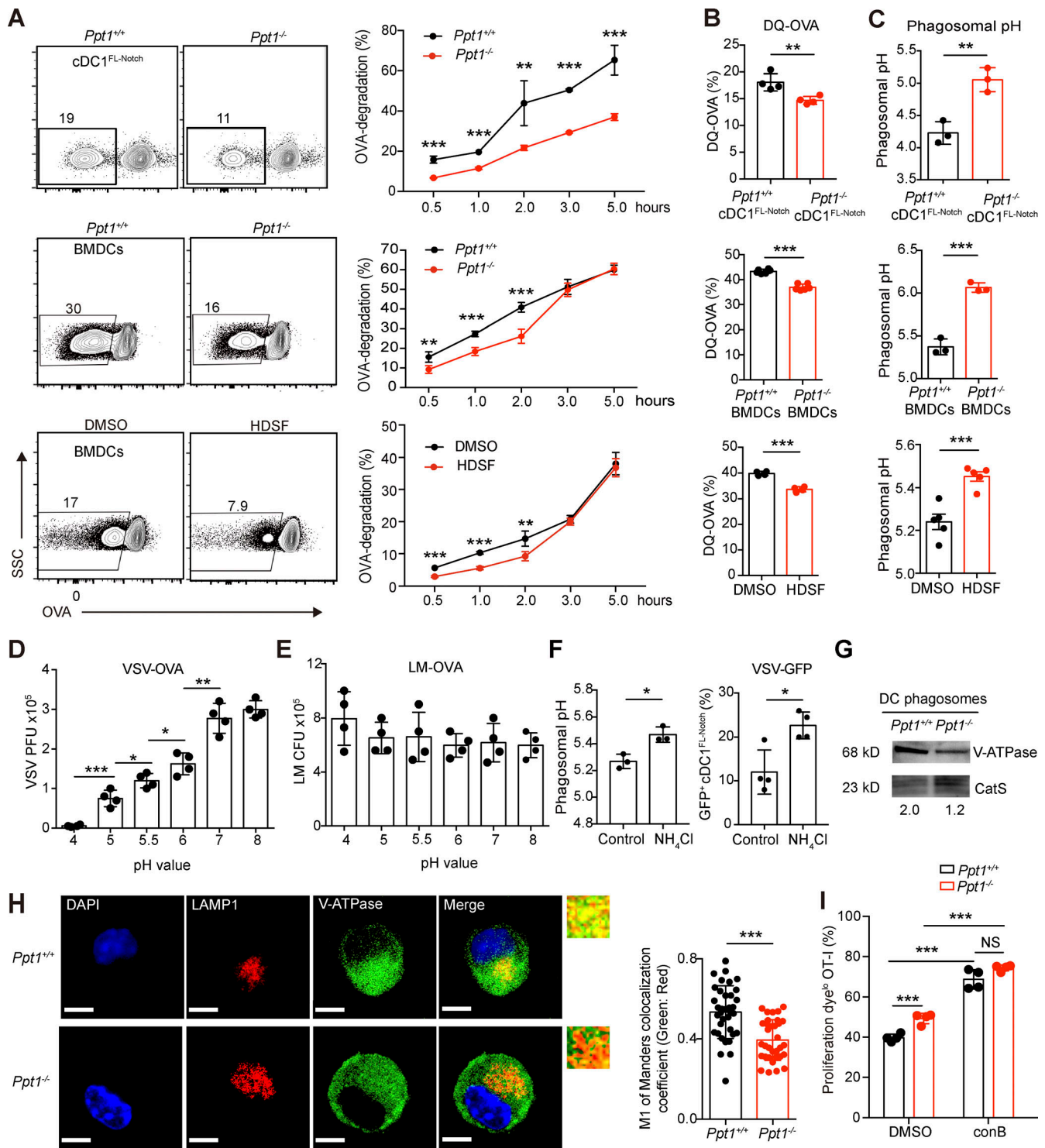


Figure 5. PPT1 promotes antigen degradation and phagosomal acidification in DCs. (A) Antigen degradation in DC phagosomes. DCs were fed OVA-associated beads for indicated times. After lysis, the supernatants containing the latex beads were collected and stained with anti-OVA antibodies. Representative FACS plots at 1 h (left) of cDC1^{FL-Notch} (top), BMDCs (center), DMSO- or HDSF-treated BMDCs (bottom), and time course (right) are shown. Data are representative of one of three independent experiments (*n* = 5 mice per group). **(B)** DQ-OVA release in DC phagosomes. BMDCs were fed DQ-OVA for 1 h. MFI of DQ-OVA in *Ppt1*^{+/+} or *Ppt1*^{-/-} cDC1^{FL-Notch} (top), BMDCs (center), and DMSO- or HDSF-treated BMDCs (bottom) are shown. Data are representative of one of three independent experiments (cDC1^{FL-Notch}, *n* = 4 mice; BMDCs, *n* = 6 mice; DMSO or HDSF, *n* = 4 mice). **(C)** DC phagosomal pH. DCs were fed AF488 OVA and pHrodo-OVA for 1 h, and the pH value was calculated according to a pH standard curve based on flow cytometry data. cDC1^{FL-Notch} (top), BMDCs (center), and DMSO- or HDSF-treated BMDCs (bottom) are shown. Data are representative of one of three independent experiments (cDC1^{FL-Notch}, *n* = 4 mice; BMDCs, *n* = 6 mice; DMSO or HDSF, *n* = 4 mice). **(D and E)** Effect of acidic pH on pathogen's infectivity. VSV-OVA (D) or LM-OVA (E) were treated with the indicated pH buffers for 30 min, quenched at pH 7.4, and then evaluated for PFU or CFU. Data are representative of one of two independent experiments (*n* = 4 technical replicates). **(F)** Effect of endosomal alkalization on VSV infection rate of cDC1s. NH₄Cl was used to increase endosomal pH on WT cDC1^{FL-Notch} (left), and

VSV-GFP⁺ cells with ddH₂O (control) or NH₄Cl treatment are shown (right). Data are representative of one of two independent experiments ($n = 4$ technical replicates). **(G)** V-ATPase V_{1a} protein expression in purified DC phagosomes. V-ATPase level was measured by Western blotting from purified BMDC phagosomes. CatS is used as loading control. Gray area ratio of vATPase over CatS is shown below. Data are representative of one of two independent experiments (sample from three pooled mice). **(H)** V-ATPase V_{1a} distribution on LAMP1⁺ endosomes. Confocal microscopy was performed using *Ppt1*^{+/+} or *Ppt1*^{-/-} BMDCs from chimeras with the indicated antibodies, and representative images (l) and the colocalization coefficient of LAMP1 and V-ATPase (right) are shown. Bars, 5 μ m (all panels). Data are representative of one of six independent experiments ($n = 35$ cell images counted randomly per group). **(I)** Inhibition of crosspriming by V-ATPase inhibitor conB. DMSO or ConB was added along with OVA-associated beads to *Ppt1*^{+/+} or *Ppt1*^{-/-} BMDCs. The percentages of Cell Proliferation Dye^{lo} CD44⁺ OT-I cells are shown. Data are representative of one of two independent experiments ($n = 4$ mice per group). All data are shown as mean \pm SD, and P values were calculated by two-way Student's *t* test (*, $P < 0.05$; **, $P < 0.01$; ***, $P < 0.001$).

to dissect the regulation of PPT1 by TLR and cytokine signaling pathways. Additionally, the transcription factors TFEB and WDFY4 also act as key antigen cross-presentation switches in DCs (Samie and Cresswell, 2015; Theisen et al., 2018). Further studies are needed to determine whether TFEB or WDFY4 controls PPT1 transcription.

Although PPT1 is known to depalmitoylate lysosomal proteins, its direct substrates or target proteins in DCs are completely unknown. First, since we found that PPT1 suppresses antigen retention and cross-presentation, the downstream targets of PPT1's enzymatic activity could be key proteins involved in antigen cross-presentation. Many Rab GTPase proteins, such as Rab27a, Rab32, Rab34, and Rab43, are involved in antigen presentation (Jancic et al., 2007; Alloatti et al., 2015; Kretzer et al., 2016; Li et al., 2016). Hence, we speculate that PPT1 might directly depalmitoylate Rab GTPases to regulate antigen presentation in DCs. In addition, phagosomal proteins directly regulating endosomal pH, such as V-ATPase or NOX2, could also be direct targets of PPT1. In neurons, V-ATPase has been shown to require palmitoylation for interaction with adaptor protein-2 and -3, respectively, for trafficking to the lysosomal membrane (Bagh et al., 2017). Second, since we found that PPT1 controls DC viral resistance, PPT1 might directly depalmitoylate viral antigens and thus suppress viral propagation. Many viral envelope proteins, including those of VSV and the influenza virus, require palmitoylation for entry, budding, and assembly (Veit, 2012). However, depalmitoylation of viral proteins could still be achieved by cytosolic acyl protein thioesterase 1, which exerts exactly the same enzymatic function as PPT1 (Salaun et al., 2010). Quantitative proteomics or specific biochemical studies, such as S-acylated proteins resin-assisted capture assay, should be conducted to confirm the possible palmitate acetylation sites in key proteins involved in cross-presentation and viral infection (Forrester et al., 2011).

Upon priming by DCs, naive CD8⁺ T cells differentiate into short-lived effector and long-lived memory subsets (Kaech and Cui, 2012). In peripheral tissue, T_{RM} (CD69⁺ CD103⁺) cells constitute a phenotypically separate lineage that is crucial for barrier immunity as well as the antitumor response (Sheridan and Lefrançois, 2011; Mackay et al., 2013; Milner et al., 2017; Amsen et al., 2018). KLRG1, along with IL-7R α (CD127), have been used extensively as markers to identify effector CD8⁺ T cells with differential effector functions, migratory properties, long-term survival and multilineage memory potential (Joshi et al., 2007). Although KLRG1⁺ IL-7R α ⁻ cells are thought to possess lower memory potential than KLRG1⁺ IL-7R α ⁺ or KLRG1⁻ IL-7R α ⁺ cells, these memory precursor subsets possess considerable heterogeneity and

plasticity (Kaech and Wherry, 2007). A recent study indicated that KLRG1⁺ IL-7R α ⁻ cells are able to differentiate into all memory subsets (including T_{RM}) and are highly effective in mounting antiviral and antitumor responses (Herndler-Brandstetter et al., 2018). Accordingly, we found that PPT1-deficient cDC1s produced more IL-12, primed more KLRG1⁺ effectors in nonlymphoid tissue, and formed more tissue-resident effector and memory cells. Thus, the enhanced T cell response in PPT1-deficient mice could be due to a combination of more cytotoxic KLRG1⁺ effectors in nonlymphoid tissue and their subsequent conversion into T_{RM} cells. Our study supports the theory that the KLRG1⁺ IL-7R α ⁻ effector subset could differentiate into T_{RM} cells.

cDC1s had been shown to crossprime naive CD8⁺ T cells into differential memory subsets during secondary infections with LM and several viruses (Alexandre et al., 2016). Recent studies showed that cDC1s were required in the optimal priming of naive CD8⁺ T cells into CD8⁺ T_{RM} cell subsets during vaccinia virus and influenza infections (Iborra et al., 2012, 2016). Although several stimulatory signals such as IL-12 had been implicated in the cross-priming of T_{RM} cells, cDC1-specific factors that regulate this process remain poorly understood (Iborra et al., 2016). Here we demonstrated that PPT1 directs the crosspriming of naive CD8⁺ T cells into tissue-resident effectors and memory T cells in tumors, bacterial infections, and chronic viral infections. Our results further support and clarify the molecular mechanism that enables cDC1 to crossprime naive CD8⁺ T cells into CD8⁺ T_{RM} cell subsets.

Our study joins a growing number of publications suggesting that the immune system may play a direct role in LSDs (Boustany, 2013). Certain LSD-associated mutations, such as lysosomal cysteine cathepsins, have been associated with macrophage dysfunction in response to *Mycobacterium tuberculosis* (Berg et al., 2016). Our results suggest that there could be CD8⁺ T cell-mediated pathologies in PPT1-deficient mice or infantile neuronal ceroid lipofuscinosis patients. On the other hand, targeting PPT1 could be a promising therapy to treat intracellular microbial infections such as *M. tuberculosis*, as well as cancer. Recently, a drug screen of lysosomal inhibitors identified PPT1 as an effective anticancer therapeutic target (Rebecca et al., 2017). Our results imply that the antitumor effect of PPT1 inhibitors could be attributed largely to PPT1's role in cDC1s. In addition, small-molecule PPT1 inhibitors are capable of breaching the blood-brain barrier and, therefore, may cause considerable damage to the central nervous system. Both neurological and immunological systems should be evaluated for any potential therapies targeting PPT1.

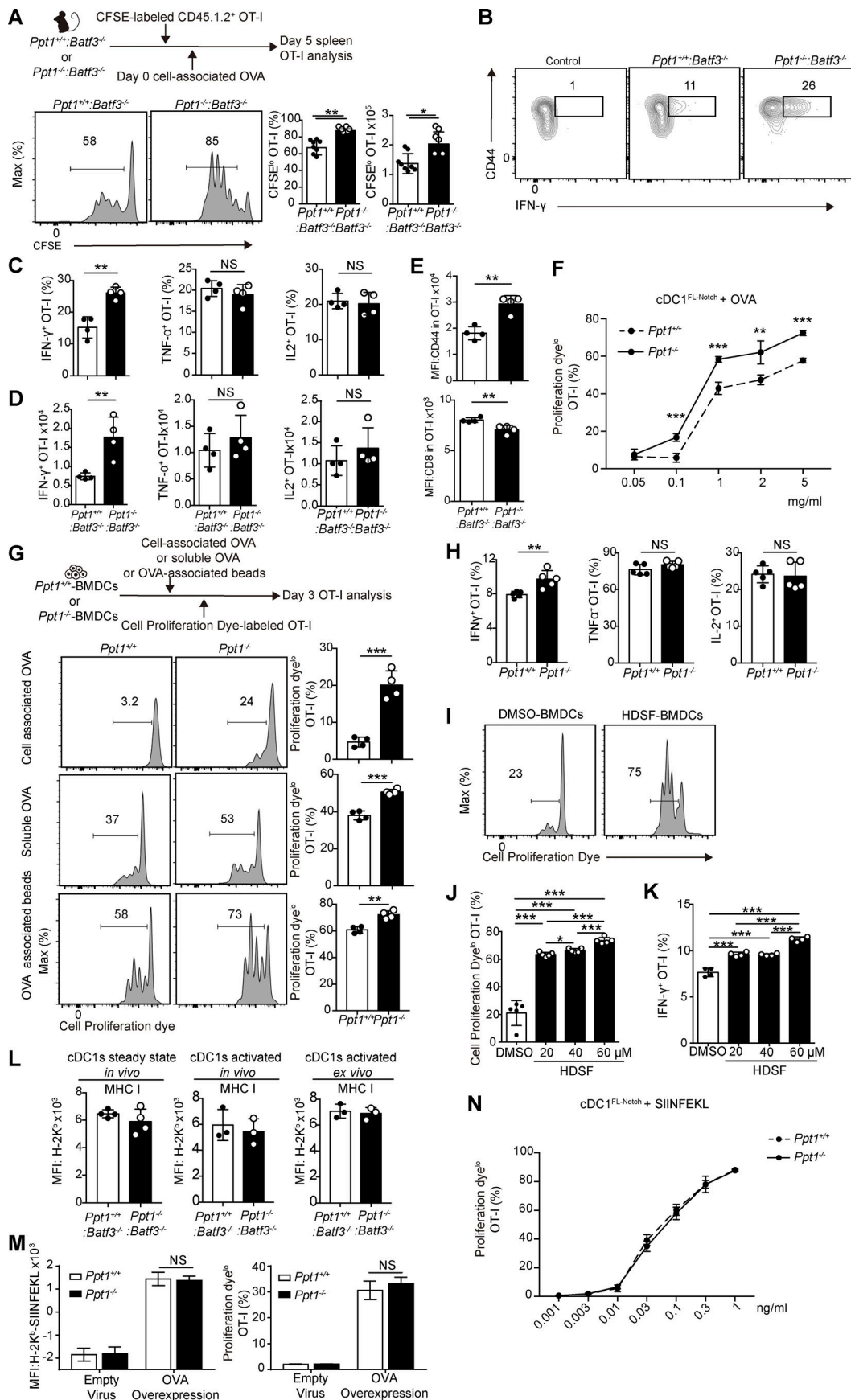


Figure 6. PPT1 suppresses antigen cross-presentation in vivo and in vitro. (A) Splenic OT-I proliferation measured by CFSE. *Ppt1^{+/+}:Batf3^{-/-}* or *Ppt1^{-/-}:Batf3^{-/-}* chimeras were injected with CFSE-labeled CD45.1.2⁺ OT-I T cells and then injected with cell-associated OVA the next day. Mice were analyzed 5 d later. Representative FACS plot (left, gated on live CD8 α^+ CD44 $^+$ CD45.1.2 $^+$), CFSE $^{\text{lo}}$ percentages (center), and cell numbers (right) are shown. Data are representative of one of five independent experiments ($n = 4$ mice per group). (B–D) Cytokine production of splenic OT-I cells. Representative FACS plots (B, gated on live CD8 α^+ CD45.1.2 $^+$ cells) are shown. Percentages of cytokine-producing OT-I cells (IFN- γ , left; TNF- α , center; and IL-2, right) and cell numbers (D) are shown. Data are representative of one of five independent experiments ($n = 4$ mice per group). (E) Expression of activation markers on splenic OT-I cells. MFI of CD44 (top) and CD8 α (bottom) are shown. Data are representative of one of five independent experiments ($n = 4$ mice per group). (F) Crosspriming by cDC1 $^{\text{FL-Notch}}$. *Ppt1^{+/+}* or *Ppt1^{-/-}* cDC1 $^{\text{FL-Notch}}$ from chimeras were fed with indicated OVA concentrations, and OT-I proliferation was measured by Proliferation dye. Data are representative of one of two independent experiments ($n = 3$ mice per group). (G) Crosspriming by BMDCs. *Ppt1^{+/+}* or *Ppt1^{-/-}* BMDCs from chimeras were fed the indicated exogenous antigens. Representative FACS plot (left, gated on live CD8 α^+ CD45.1 $^+$) of *Tap1^{-/-}* cell-associated OVA (top), soluble OVA (center), or OVA-associated beads (bottom). Percentages of Cell Proliferation Dye $^{\text{lo}}$ CD44 $^+$ OT-I cells (right) are shown. Data are representative of one of three independent experiments ($n = 4$ mice per group). (H) Cytokine production of crossprimed OT-I cells. *Ppt1^{+/+}* or *Ppt1^{-/-}* BMDCs from chimeras were fed with *Tap1^{-/-}* cell-associated OVA. Percentages of cytokine-producing OT-I cells (IFN- γ , left; TNF- α , center; and IL-2, right) are shown. Data are representative of one of three independent experiments ($n = 4$ mice per group). (I and J) OT-I proliferation measured by Cell Proliferation Dye. DMSO or HSDF-treated WT BMDCs were fed with *Tap1^{-/-}* cell-associated OVA. Representative FACS plot (I) and Cell Proliferation Dye $^{\text{lo}}$ OT-I cell percentages (J) are shown. Data are representative of one of three independent experiments ($n = 4$ mice per group). (K) IFN- γ production by OT-I cells. DMSO- or HSDF-treated WT BMDCs were fed with *Tap1^{-/-}* cell-associated OVA, and OT-I cells were stimulated with SIINFEKL. Data are representative of one of three independent experiments ($n = 5$ mice per group). (L) MHC class I expression on cDC1s. H2-K $^{\text{b}}$ expression was measured by FACS on naive splenic cDC1s (left), during LM-OVA infection (center), and LPS-activated (right) cDC1s from *Ppt1^{+/+}:Batf3^{-/-}* or *Ppt1^{-/-}:Batf3^{-/-}* chimeras. Data are representative of one of two independent experiments ($n = 3$ mice). (M) Effect of PPT1 on endogenous MHC class I presentation. WT BMDCs were transduced with empty or OVA-expressing retroviruses and then incubated with OT-I cells. MFI of H-2K $^{\text{b}}$ -SIINFEKL (25.D1.16, left) and OT-I proliferation (right) are shown ($n = 3$ technical replicates). Data are representative of one of two independent experiments. (N) Direct MHC I antigen presentation by cDC1 $^{\text{FL-Notch}}$. *Ppt1^{+/+}* or *Ppt1^{-/-}* cDC1 $^{\text{FL-Notch}}$ from chimeras were pulsed with indicated concentrations of SIINFEKL and then incubated with CFSE-labeled CD45.1.2 $^+$ OT-I cells. Data are representative of one of two independent experiments ($n = 3$ mice per group). All data are shown as mean \pm SD, and P values were calculated by two-way Student's *t* test (*, $P < 0.05$; **, $P < 0.01$; ***, $P < 0.001$).

Finally, we obtained consistent results in cross-presenting cDC1s and BMDCs (both GM-CSF and FLT3L-derived) *in vitro* and *in vivo*, suggesting that PPT1 belongs to an antigen presentation pathway conserved in divergent cross-presenting DC types. Our results suggest that the dynamic expression of PPT1 in cross-presenting DCs serves dual functions of viral resistance and efficient CD8 $^+$ T cell crosspriming. The modulation of PPT1 by therapeutics represents a flexible tool to manipulate the immune response in diverse pathological conditions.

Materials and methods

Mice

C57BL/6J, BALB/cJ (BALB/c), B6.SJL-*Ptprc^aPepc^b*/BoyJ (CD45.1 $^+$), B6.129S2-*Tap1^{tm1Atp}*/J (*Tap1^{-/-}*), C57BL/6-Tg(*TcraTcrb*)1100Mjb/J (OT-I), B6.129S6-*Ppt1^{tm1Hof}*/SopJ, (*Ppt1^{-/-}*), and B6.129S(C)-*Batf3^{tm1Kmm}*/J (*Batf3^{-/-}*) mice were purchased from the Jackson Laboratory. B6.129S6-*Ppt1^{tm1Hof}*/SopJ (*Ppt1^{-/-}*) mice were backcrossed for ≥ 10 generations with C57BL/6J. Mice designated as WT or CD45.1 $^+$ were derived from in-house breeding of C57BL/6 or B6.SJL-*Ptprc^aPepc^b*/BoyJ strains. Age- and sex-matched mice 6–12 wk of age were used. All mice were bred and maintained in specific pathogen-free conditions at GemPharmatech Co., Ltd., and BSL3 facilities at Sun Yat-sen University, according to the institutional guidelines and protocols approved by the Animal Ethics Committee of Sun Yat-sen University, Guangzhou, Guangdong, China.

Generation of chimeras

For *Ppt1^{-/-}* chimeras, CD45.1 $^+$ mice were lethally irradiated with 950 rad and then injected i.v. with 1×10^6 bone marrow cells harvested from *Ppt1^{+/+}* or *Ppt1^{-/-}* littermates. The mice were fed antibiotics for 2 wk and then rested for at least an additional 4 wk to allow reconstitution of immune cells. For *Ppt1^{+/+}:Ppt1^{-/-}*

chimeras, CD45.1.2 $^+$ mice were lethally irradiated with 950 rad and then injected i.v. with 1×10^6 bone marrow cells harvested from age- and sex-matched WT CD45.1 $^+$ and CD45.2 $^+$ *Ppt1^{-/-}* mice at the ratio of 1:1. For *Ppt1^{+/+}* or *Ppt1^{-/-}:Batf3^{-/-}* chimeras, CD45.1 $^+$ mice were lethally irradiated with 950 rad and then injected i.v. with 1×10^6 bone marrow cells harvested from *Ppt1^{+/+}* or *Ppt1^{-/-}* littermates, and 1×10^6 bone marrow cells were harvested from age- and sex-matched *Batf3^{-/-}* mice. The mice were fed antibiotics for 2 wk and rested for at least an additional 4 wk to allow the reconstitution of immune cells.

Immune cell isolation

To harvest immune cells from lymphoid tissue, organs were minced, ground up, and passed through a 70- μm nylon mesh. Erythrocytes were removed using ammonium-chloride-potassium lysis buffer (150 mM ammonium chloride, 10 mM potassium bicarbonate, and 0.1 mM EDTA). The cells were counted using Beckman Coulter CytoFlex. Before sorting, DCs were enriched with CD11c microbeads (Miltenyi Biotec). For peripheral tissues, organs were digested in collagenase D (Roche) and DNase I (Sigma-Aldrich) for 1 h at 37°C with stirring in PBS. Liver immune cells were separated using a Percoll gradient (Sigma-Aldrich). For isolation of intraepithelial lymphocytes, the small intestine was removed, Peyer's patches were excised, and the intestine was cut longitudinally and then laterally into 0.5–1-cm 2 pieces. Tissues were incubated with 0.154 mg/ml dithioerythritol in 10% HBSS/Hepes bicarbonate buffer for 30 min at 37°C, and then with 100 U/ml type I collagenase in RPMI 1640, 5% FBS, 2 mM MgCl $_2$, and 2 mM CaCl $_2$ for 30 min at 37°C with stirring at 250 rpm. After enzymatic treatment, tissues were further dissociated over a 70- μm nylon cell strainer. For isolation of lymphocytes, single-cell suspensions were separated using a 44/67% Percoll (Sigma-Aldrich) density gradient.

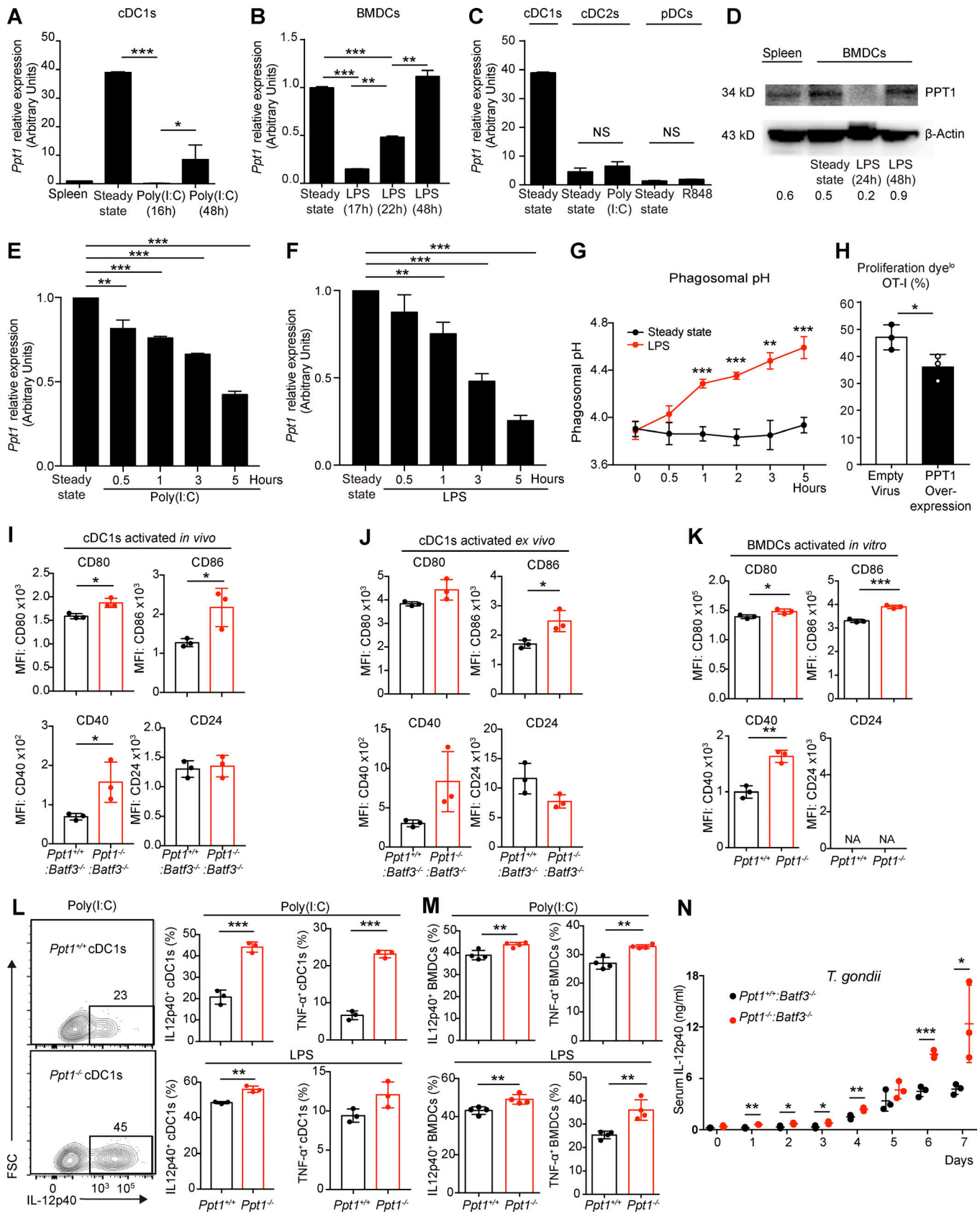


Figure 7. **Rapid down-regulation of PPT1 in activated cDC1s facilitates efficient crosspriming.** (A) *Ppt1* mRNA expression in activated cDC1s. FACS sorted WT cDC1s were stimulated with poly(I:C), and *Ppt1* transcript was measured by qPCR. Data are combined results of three independent experiments (n = relative values from three independent runs). (B) *Ppt1* mRNA expression in activated BMDCs. WT BMDCs were stimulated with LPS, and *Ppt1* transcript was

measured by qPCR. Data are combined results of three independent experiments (n = relative values from three independent runs). **(C)** *Ppt1* mRNA expression in other activated DCs. Indicated FACS-sorted WT populations were stimulated, and *Ppt1* transcript was measured by qPCR. Data are combined results of three independent experiments (n = relative values from three independent runs). **(D)** PPT1 protein expression in activated BMDCs. WT BMDCs were stimulated with LPS, and PPT1 expression was measured by Western blotting. β -Actin was used as loading control. Gray area ratio of PPT1 over β -actin is shown below. Data are representative of one of two independent experiments (sample from three pooled mice). **(E and F)** PPT1 down-regulation after DC activation. WT BMDCs were stimulated with poly(I:C) (E) or LPS (F), and *Ppt1* transcript was measured at indicated time points by qPCR. Data are combined results of three independent experiments (n = relative values from three independent runs). **(G)** Phagosomal alkalization after DC activation. WT BMDCs were stimulated with LPS, and then fed with AF488-OVA and pHrodo-OVA. Phagosomal pH was then calculated at indicated time points accordingly. Data are representative of one of two independent experiments (n = 3 mice per group). **(H)** Crosspriming by DCs with PPT1 overexpression. WT BMDCs were transduced with empty or PPT1-overexpressing retroviruses, then fed with OVA and OT-I cells. Data are representative of one of two independent experiments (n = 3 technical replicates). **(I)** Costimulatory signals by activated cDC1s in vivo. *Ppt1*^{+/+}:*Batf3*^{-/-} or *Ppt1*^{-/-}:*Batf3*^{-/-} chimeras were infected with LM-OVA, and then splenic cDC1s (gated on live CD11c^{hi} MHC II⁺ XCR1⁺ CD172a⁻) were analyzed at day 5. MFI of CD80, CD86, CD40, and CD24 are shown. Data are representative of one of three independent experiments (n = 3 mice per group). **(J)** Costimulatory signals by activated cDC1s ex vivo. Splenic cDC1s (gated on live CD11c^{hi} MHC II⁺ XCR1⁺ CD172a⁻) were sorted from *Ppt1*^{+/+}:*Batf3*^{-/-} or *Ppt1*^{-/-}:*Batf3*^{-/-} chimeras and then activated in vitro with LPS for 18 h. MFI of CD80, CD86, CD40, and CD24 are shown. Data are representative of one of three independent experiments (n = 3 mice per group). **(K)** Costimulatory signals by activated BMDCs in vitro. Surface molecule expression was analyzed on *Ppt1*^{+/+} or *Ppt1*^{-/-} BMDCs from chimeras activated with LPS for 18 h. MFI of CD80, CD86, CD40, and CD24 are shown. Data are representative of one of three independent experiments (n = 3 mice per group). **(L)** Cytokine production by activated cDC1s. FACS-sorted cDC1s from *Ppt1*^{+/+}:*Batf3*^{-/-} or *Ppt1*^{-/-}:*Batf3*^{-/-} chimeras were activated with poly(I:C) or LPS for 18 h, then analyzed by FACS intracellular staining. Representative FACS plot of poly(I:C)-stimulated cDC1s (IL-12p40, left), percentages of IL-12p40, and TNF- α production with poly(I:C; right, top) or LPS (right, bottom) are shown. Data are representative of one of three independent experiments (n = 3 mice per group). **(M)** Cytokine production by activated BMDCs. *Ppt1*^{+/+} or *Ppt1*^{-/-} BMDCs from chimeras were activated with poly(I:C) or LPS for 18 h, then analyzed by intracellular IL-12p40 and TNF- α FACS staining. Data are representative of one of three independent experiments (n = 3 mice per group). **(N)** Serum IL-12p40 level during *T. gondii* infection. *Ppt1*^{+/+}:*Batf3*^{-/-} or *Ppt1*^{-/-}:*Batf3*^{-/-} chimeras were infected with *T. gondii*, and serum IL-12p40 was measured by ELISA on indicated days. Data are representative of one of two independent experiments (n = 3 mice per group). All data are shown as mean \pm SD, and P values were calculated by two-way Student's *t* test (*, $P < 0.05$; **, $P < 0.01$; ***, $P < 0.001$).

Flow cytometry

Flow cytometry was performed on Beckman Coulter CytoFlex and analyzed using FlowJo software (TreeStar). Mean fluorescence intensity (MFI) was calculated by genomic mean in FlowJo. Cell-sorting experiments were conducted on a BD Aria II. Staining was performed at 4°C in the presence of Fc block (Clone 2.4G2; BD) and FACS buffer (PBS, 0.5% BSA, 2 mM EDTA, and 0.1% sodium azide). In the case of intracellular cytokine staining, brefeldin A (eBioscience) was added with peptide (10 nM SIINFEKL for OT-I cells) or TLR ligands (for BMDCs) for 4–8 h before staining with the intracellular staining kit (eBioscience). The following antibodies were all purchased from eBioscience unless otherwise indicated: anti-CD8 α (53-6.7), IL-2 (JES6-5H4), CD69 (H1.2F3), TNF- α (MP6-XT22), CD45.1 (A20), CD44 (IM7), CD80 (16-10A1), IFN- α (RMMA-1), CD11C (N418), Clec9A (42D2), IFN- γ (XMG1.2), MHC II (M5-114.15.2), CD24 (M1-69), CD86 (GL1), PD-L1 (NIH5), CD127 (A7R34), XCR1 (ZET; BioLegend), CD103 (2E7), KLRG1 (2F1), IL-12p40 (C17.8), PD-1(J43), CD40 (IC40), SIINFEKL-peptide bound to H2-K^b (25.D1.16), LCMV gp33-H-2D^b (gp33-41; MBL), and H-2K^b (AF6-88.5.5.3). MFI were calculated by genomic mean.

BMDCs

As previously described (Helft et al., 2015), in short, 10 \times 10⁶ bone marrow cells per well were cultured in tissue culture-treated 6-well plates in 4 ml of RP10 (RPMI 1640 supplemented with glutamine, penicillin, streptomycin, and 2-mercaptoethanol; all from Invitrogen), 10% heat-inactivated fetal calf serum (Source BioSciences), and GM-CSF (20 ng/ml; Peprotech). Half of the medium was removed at day 2, and new medium supplemented with GM-CSF (40 ng/ml) and warmed at 37°C was added. The culture medium was entirely discarded at day 3 and replaced with fresh warmed medium

containing GM-CSF (20 ng/ml). For BMDC activation, 10 μ g/ml poly(I:C) (HMW; Invitrogen) or 5 μ g/ml LPS (*Escherichia coli* O26:B6; eBioscience) was used at the indicated time points. BMDCs were gated as live⁺ CD11b⁺ MHCII⁺ CD11c⁺ cells.

DC^{FL-Notch} culture

As previously described (Kirkling et al., 2018), single-cell suspensions of primary murine BM cells were suspended in RPMI 1640 medium supplemented with 10% FCS, 1% L-glutamine, 1% sodium pyruvate, 1% MEM with nonessential amino acids, 1% penicillin/streptomycin, 55 μ M 2-mercaptoethanol, and 10% supernatant from cultured B16-FLT3L cell line (DC medium). Cells were plated at 2 \times 10⁶ cells per well in 2 ml of DC medium in 24-well plates and cultured at 37°C in a humidified incubator at 5% CO₂. On day 3 of differentiation, half of the volume of cells in DC medium from each well was transferred to a single well containing a monolayer of mitomycin-treated OP9-DL1 cells in 24-well plates. Cell cultures were analyzed on day 7. cDC1^{FL-Notch} were gated as live⁺ DEC205⁺ CD24⁺ CD8 α ⁺ CD11b⁻ MHCII⁺ CD11c⁺ cells.

Retroviral transduction of BMDCs

Phoenix packaging cells (#CRL-3214; ATCC) were transfected with 20 μ g of the plasmid pCL-Eco (#25099; Addgene) and 16 μ g of pMXs-PPT1, pMXs-OVA (cloned from Addgene #25099), or empty vector pMXs with 90 μ l transfecting reagent polyethylenimine (23966-1; Polysciences) at 1 mg/ml in a 10-cm culture dish. After 48 h, the supernatant containing retrovirus was harvested and filtered. For BMDC retroviral transduction, on days 1 and 2, 2 ml retroviral supernatant was added, and cells were spin-infected (2,500 rpm) for 90 min at room temperature. On day 3, fresh medium was added to the cells, and they were cultured for two more days. All retroviral transduction rate was >70% as measured by GFP with FACS.

In vivo antigen cross-presentation assays with cell-associated OVA

As previously described (Moore et al., 1988), in short, BALB/c or *Tap1*^{-/-} splenocytes were loaded with OVA by osmotic shock. Cells were incubated in hypertonic medium (0.5 M sucrose, 10% polyethylene glycol, and 10 mM Hepes in RPMI 1640, pH 7.2) containing 10 mg/ml OVA for 10 min at 37°C, and then pre-warmed hypotonic medium (40% H₂O and 60% RPMI 1640) was added for an additional 2 min at 37°C. After washing and irradiation (1,350 rad), OVA-loaded cells were injected into mice that had been injected i.v. 24 h earlier with CFSE-dyed OT-I cells.

In vitro antigen cross-presentation assays

As previously described (Alloatti et al., 2015), in short, BMDCs were pulsed overnight with OVA protein (5 mg/ml) or OVA conjugated to 3- μ m latex beads (Polyscience): *Tap1*^{-/-} cell-associated OVA (BMDC:cell-associated OVA = 1:5). The cells were cocultured with OVA-specific OT-I T cells stained with CFSE or cell proliferation dye for 10 min at 37°C at a 1:2 ratio in 24-well plates. After 3 d, OT-I T cell proliferation was analyzed by flow cytometry.

In vivo and in vitro infection models

In vivo

As previously described (Yang et al., 2011), in short, at day 0, 1×10^5 OT-I cells were injected i.v. into mice. For LM-OVA infection, LM-OVA was grown in Tryptic soy broth (TSB) medium to an OD₆₀₀ of ~0.25, diluted in PBS, and injected i.v. (8×10^3 CFU) in a volume of 0.2 ml per mouse. After 5 d, the mice were analyzed. Splenic cDC1s were FACS sorted and plated in TSB solid medium overnight at 37°C. For VSV-OVA infection, 1×10^6 PFU were diluted in PBS and injected i.v. For the VSV-PFU plaque-forming assay, Vero cells were plated in 6-well plates. Next, 100 μ l of the samples were added to the Vero cell monolayers. After incubating the plates for 60–90 min in a humidified 37°C 5% CO₂ incubator with occasional rocking every 20–30 min, the agarose overlay was prepared by combining equal volumes of 2 \times MEM and 1% agarose solution in water. To each monolayer, 3 ml agarose overlay was added. Plates were incubated for 2 d at 37°C with 5% CO₂. They were then stained with 1 ml of a 1:10,000 dilution of neutral red (from a 1% aqueous solution) made up in 1:1 2 \times MEM and 1% agarose and incubated overnight at 37°C in 5% CO₂. For the LM-CFU colony-forming assay, 100- μ l samples were added to TSB solid medium and incubated overnight at 37°C. For LCMV CLI3 infection, 1×10^6 PFU were diluted in PBS and injected i.p. into mice. Lung peribronchial inflammation scoring was as previously described (Myou et al., 2003): 0, normal; 1, few cells; 2, a ring of inflammatory cells one cell layer deep; 3, a ring of inflammatory cells two to three cells deep; 4, a ring of inflammatory cells four cells deep. For parasitic infections, *T. gondii* (RH strain) tachyzoites were grown in human foreskin fibroblast culture. 200 freshly egressed tachyzoites were filtered, counted, and injected i.v. into mice.

In vitro

For VSV-GFP infection, BMDCs and cDC1^{FL-Notch} were cultured as described above. Virus (multiplicity of infection: 16) only or

with NH₄Cl (3 mM; Sigma-Aldrich) was added into culture medium. After 24-h incubation, cells were analyzed. For VSV-GFP and VSV-OVA mixed infection, 293T cells were infected by VSV-GFP and VSV-OVA, harvested, washed three times in cold 1 \times PBS to remove cell lysate, and cocultured with cDC1^{FL-Notch} for 24 h. Then GFP⁺ cDC1^{FL-Notch} and GFP⁻ cDC1^{FL-Notch} were sorted and fixed with 0.008% (vol/vol) glutaraldehyde for 10 min at 4°C and washed twice with 0.2 M glycine and once again with 1 \times PBS. Resuspended cells were then cocultured with OT-I separately. OT-I proliferation was analyzed on day 3. For the LM/VSV infectivity pH assay, VSV-OVA or LM-OVA were treated with 2-(*N*-morpholino)ethanesulfonic acid (MES) medium (including 5 mM NaCl, 115 mM KCl, 12 mM MgSO₄, 25 mM MES, 10 μ M nigericin, 10 μ M monensin, and 1% Trixon X-100), which was adjusted to the indicated pH for 30 min at 37°C. The samples were then neutralized to pH 7.4 for 10 min, and the CFU or PFU were measured.

In vivo cytotoxicity assay

As previously described (Iborra et al., 2012), in short, splenocytes were split into two populations that were labeled as a high or intermediate concentrations of CFSE and then washed. CFSE^{hi} cells were pulsed with 10 μ M CFSE, and CFSE^{int} cells were pulsed with 0.125 μ M CFSE along with 10 nM OVA peptide SIINFEKL. Pulsed CFSE^{hi} cells and CFSE^{int} cells were then mixed equally and injected i.p. into syngeneic mice. After 24 h, the peritoneal lavage was obtained and analyzed by flow cytometry to measure in vivo killing.

Tumor mouse models

The B16-F10 cell line was purchased from ATCC (CRL-6475). B16-OVA was generated in-house from ATCC stock stably transfected with plasmid containing OVA. MC38 cell line was purchased from Kerablast (ENH204). Authentication was provided by ATCC or Kerablast. The cell lines were confirmed to be negative for mycoplasma contamination by PCR. B16-OVA and MC38 were cultured at 37°C in RPMI with 10% FCS. 5×10^5 tumor cells were injected s.c. with 100 μ l in each flank. Tumor size was determined on the indicated days by the following formula: length \times width \times width \times 0.5.

FITC uptake assay

As previously described (Tussiwand et al., 2015), in short, after shaving the hair on the abdomen, mice were treated with 40 μ l of 1% hapten FITC (Sigma-Aldrich) that had been diluted in 1:1 dibutyl phthalate/acetone as antigen. 24 h later, the cells of skin-draining lymph nodes were stained for flow cytometric analysis.

BMDC adoptive transfer

For LM BMDC treatment, at day 0, 1×10^5 OT-I were injected into the mice. The mice were infected with 8,000 CFU LM-OVA on day 1. The next day, 2×10^5 DMSO- or HDSF-treated BMDCs cocultured with OVA were transferred i.v. into the mice. For the tumor BMDC treatment model, soluble OVA were added to BMDCs at day 5. The next day, 2×10^6 BMDCs were injected to mice i.v. After 9 d, 1×10^6 B16-OVA cells were injected into mice

s.c. Tumor size was determined on the indicated days by the following formula: length × width × width × 0.5.

Phagosomal protein degradation assay

As previously described (Samie and Cresswell, 2015), in short, BMDCs were incubated at 37°C for 25 min with latex beads (Polyscience) that had been conjugated to OVA and washed once with cold 2% BSA in PBS. After removing the uningested beads by centrifugation, the cells were incubated for the indicated durations, disrupted in lysis buffer (50 mM Tris-HCl, pH 7.4, 150 mM NaCl, 0.5% NP-40, 1 mM dithiothreitol [DTT], and 200× protease inhibitor cocktail) and centrifuged at 900 rpm for 5 min at 4°C. The supernatants containing the latex beads were collected and stained with anti-OVA antibody. The OVA protein remaining on the surface of the beads was then analyzed by flow cytometry.

Phagosomal pH assay

As previously described (Samie and Cresswell, 2015), in short, 3- μ m latex beads were coated overnight with OVA conjugated to the pH-sensitive dye pHrodo-OVA (Sigma-Aldrich) or with the pH-insensitive dye Alexa Fluor 488 (Sigma-Aldrich) at 4°C. The next day, the beads were washed and stored in PBS. BMDCs were pulsed with the coupled beads for 25 min at 37°C and then washed with cold PBS. The cells were then incubated at 37°C for the indicated times and immediately analyzed by flow cytometry. The ratio of the MFI of one dye to that of the other was determined. The MFI values were then compared with the standard curve obtained by the resuspension of cells that had phagocytosed beads for 1 h in calibration buffer containing MES buffer (including 5 mM NaCl, 115 mM KCl, 12 mM MgSO₄, 25 mM MES, 10 μ M nigericin, 10 μ M monensin, and 1% Triton X-100) of different pH values ranging from 3 to 8 and 1% Triton X-100.

Confocal microscopy

BMDCs were placed on glass coverslips that had been treated with poly-L-lysine at room temperature for 30 min. After washing with PBS, the cells were fixed with 4% paraformaldehyde for 60 min. Paraformaldehyde-fixed cells were permeabilized with 0.2% Triton X-100 in PBS. After blocking with 5% goat serum, the cells were incubated with primary antibodies overnight at 4°C, followed by secondary antibodies. The primary antibodies used were ATP6V1a (ab137574, dilution 1:100; Abcam) and LAMP1 (sc-19992, dilution 1:200; Santa Cruz Biotechnology). Cells were mounted with DAPI, and fluorescence was visualized with a Nikon C2 confocal microscope. The image was processed with Imaris 8.4 software. Mander's colocalization coefficient was calculated using ImageJ (National Institutes of Health). Mander's M1 was used to determine the degree of the green channel that colocalized with the red channel.

Phagosome purification

BMDCs were incubated at a ratio of 1:5 with 3- μ m latex beads for 1 h at 37°C. Cells were then disrupted in 500 μ l homogenization buffer (containing 8% sucrose in PBS, 3 mM imidazole, 2 mM DTT, 5 μ g/ml DNase, and 2× protease inhibitor cocktail). The

total cell volume was taken in a syringe harboring a 22-gauge needle. After cell viability reached ~70%, they were centrifuged for 4 min at 4°C. Phagosomes were removed from postnuclear supernatants and washed three times in ice-cold washing solution (10 mM Hepes, 10 mM NaCl, 110 mM KCl, 5 mM Mg₂Cl, and 2mM DTT in H₂O). Phagosomes were lysed in lysis buffer (RIPA buffer plus 2 mM DTT and 1× protease inhibitor cocktail) for 30 min at 4°C. Cellular debris was excluded by centrifuging.

Western blotting

Purified phagosomes (20 μ g) or total cell lysates (60 μ g) from BMDCs were run on SDS-PAGE with 4–12% gradient gel and then transferred. The membranes were blocked with 5% dried milk and incubated with primary antibodies overnight. After washing with PBS with Tween 20, secondary antibodies were incubated with the membranes for 1.5 h. The bands were visualized by chemical composition using ChemiDoc Touch (Bio-Rad). The gray area ratio of different bands was calculated by software from ChemiDoc Touch (Bio-Rad). The following antibodies were used: PPT1 (NIC3; GeneTex), catS (E-3; Santa Cruz Biotechnology), ATP6V1A (ab137574; Abcam), and β -actin (AC74; Sigma-Aldrich).

ELISA

Serum samples were plated on a mouse IL-12 (p40) ELISA Set (555165; BD Biosciences), and ELISA was performed according to the manufacturer's instructions.

RNA extraction and qPCR

TRIzol reagent (Thermo Fisher Scientific) and chloroform were added to homogenize single cells, followed by RNA precipitation, washing, and resuspension according to the manufacturer's protocol. The extracted RNA was used for reverse transcription according to the manufacturer's protocol (Thermo Fisher Scientific). Quantitative RT-PCR analysis was performed with SYBR Select Master Mix (Invitrogen) using StepOne Plus (Life Sciences). Primer sequences were *Ppt1* forward, 5'-TTGTGGACC CTGTCGACTCT, and reverse, 5'-GATGGTCCCCTTCCTTAGCC-3'; β -actin forward, 5'-GTGACGTTGACATCCGTAAGA-3', and reverse, 5'-GCCGGACTCATCGTACTCC-3'; LCMV NP forward, 5'-CAGAAATGTTGATGCTGGACTGC-3', and reverse, 5'-CAG ACCTTGCTTACACAG-3'; and LCMV GP forward, 5'-CATTACCTGGACTTTGTCAGACTC-3', and reverse, 5'-GCA ACTGCTGTGCCGAAAC-3'.

Statistical analysis

Statistical analysis was performed in GraphPad Prism 6 software. Comparisons between two groups were performed by the two-way Student's *t* test. A *P* value of ≤ 0.05 was considered significant: *, *P* < 0.05; **, *P* < 0.01; ***, *P* < 0.001 (two-tailed *t* test).

Online supplemental material

Fig. S1 shows the expression of *Ppt1* transcript in immune cells, as well as the generation of the chimeric mice. Fig. S2 analyzes the immune cell development in PPT1-deficient mice. Fig. S3 assesses the phagocytosis rate of PPT1-deficient DCs. Fig. S4

compares natural killer (NK) cell functions between PPT1-deficient and -sufficient chimeras. Fig. S5 analyzes different memory subsets during LM infection.

Acknowledgments

We thank Dr. Ananda W. Goldrath (University of California at San Diego, San Diego, CA) for the VSV-OVA, LM-OVA, and LCMV CL13; Dr. Margaret Kirkling (New York University, New York, NY) for OP9-DL1; and Dr. Penghui Zhou (Sun Yat-sen University Cancer Center, Guangzhou, Guangdong, China) for the B16-OVA and MC38 cell lines. We are grateful for critical reading of the manuscript by Dr. Kyla Omilusik and Dr. Ananda W. Goldrath, as well as members of the C.Y. Yang laboratory. We thank Dr. Weibin Cai for technical assistance at the animal facilities.

This research is supported by the National Key R&D Program of China (2018YFA0508300) to C.Y. Yang, the National Natural Science Foundation of China (31570863) to C.Y. Yang, the Guangdong Innovative and Entrepreneurial Research Team Program (2016ZT06S638) to C.Y. Yang, the 111 Project (grant no. B12003) to C.Y. Yang, and National Institutes of Health grant AI072571 to B. Reizis.

The authors declare no competing financial interests.

P. Ou designed and performed the experiments, analyzed the data and helped to write the manuscript. L. Wen, X. Liu, and C. Su designed and performed the experiments and analyzed the data. X. Huang, J. Huang, L. Wang, and H. Ni performed experiments. B. Reizis conceived the initial study, designed the experiments, and helped to write the manuscript. C.Y. Yang designed the experiments, oversaw the protocol logistics, analyzed and interpreted the data, and wrote the manuscript. B. Reizis and C.Y. Yang are co-senior authors and jointly supervised this work.

Submitted: 9 January 2019

Revised: 5 May 2019

Accepted: 12 June 2019

References

Accapezzato, D., V. Visco, V. Francavilla, C. Molette, T. Donato, M. Paroli, M.U. Mondelli, M. Doria, M.R. Torrisi, and V. Barnaba. 2005. Chloroquine enhances human CD8⁺ T cell responses against soluble antigens in vivo. *J. Exp. Med.* 202:817–828. <https://doi.org/10.1084/jem.20051106>

Ackerman, A.L., and P. Cresswell. 2004. Cellular mechanisms governing cross-presentation of exogenous antigens. *Nat. Immunol.* 5:678–684. <https://doi.org/10.1038/nri082>

Alexandre, Y.O., S. Ghilas, C. Sanchez, A. Le Bon, K. Crozat, and M. Dalod. 2016. XCR1⁺ dendritic cells promote memory CD8⁺ T cell recall upon secondary infections with *Listeria monocytogenes* or certain viruses. *J. Exp. Med.* 213:75–92. <https://doi.org/10.1084/jem.20142350>

Aliberti, J., O. Schulz, D.J. Pennington, H. Tsujimura, C. Reis e Sousa, K. Ozato, and A. Sher. 2003. Essential role for ICSBP in the in vivo development of murine CD8 α + dendritic cells. *Blood.* 101:305–310. <https://doi.org/10.1182/blood-2002-04-1088>

Alloati, A., F. Kotsias, A.M. Pauwels, J.M. Carpier, M. Jouve, E. Timmerman, L. Pace, P. Vargas, M. Maurin, U. Gehrmann, et al. 2015. Toll-like Receptor 4 Engagement on Dendritic Cells Restrains Phago-Lysosome Fusion and Promotes Cross-Presentation of Antigens. *Immunity.* 43:1087–1100. <https://doi.org/10.1016/j.immuni.2015.11.006>

Amsen, D., K.P.J.M. van Gisbergen, P. Hombrink, and R.A.W. van Lier. 2018. Tissue-resident memory T cells at the center of immunity to solid tumors. *Nat. Immunol.* 19:538–546. <https://doi.org/10.1038/s41590-018-0114-2>

Bagh, M.B., S. Peng, G. Chandra, Z. Zhang, S.P. Singh, N. Pattabiraman, A. Liu, and A.B. Mukherjee. 2017. Misrouting of v-ATPase subunit V0a1 dysregulates lysosomal acidification in a neurodegenerative lysosomal storage disease model. *Nat. Commun.* 8:14612. <https://doi.org/10.1038/ncomms14612>

Berg, R.D., S. Levitte, M.P. O'Sullivan, S.M. O'Leary, C.J. Cambier, J. Cameron, K.K. Takaki, C.B. Moens, D.M. Tobin, J. Keane, and L. Ramakrishnan. 2016. Lysosomal Disorders Drive Susceptibility to Tuberculosis by Compromising Macrophage Migration. *Cell.* 165:139–152. <https://doi.org/10.1016/j.cell.2016.02.034>

Bougnères, L., J. Helft, S. Tiwari, P. Vargas, B.H. Chang, L. Chan, L. Campisi, G. Lauvau, S. Hugues, P. Kumar, et al. 2009. A role for lipid bodies in the cross-presentation of phagocytosed antigens by MHC class I in dendritic cells. *Immunity.* 31:232–244. <https://doi.org/10.1016/j.immuni.2009.06.022>

Boustany, R.M. 2013. Lysosomal storage diseases--the horizon expands. *Nat. Rev. Neurol.* 9:583–598. <https://doi.org/10.1038/nrneurol.2013.163>

Bowie, A.G., and L. Unterholzner. 2008. Viral evasion and subversion of pattern-recognition receptor signalling. *Nat. Rev. Immunol.* 8:911–922. <https://doi.org/10.1038/nri2436>

Breton, G., S. Zheng, R. Valieris, I. Tojal da Silva, R. Satija, and M.C. Nusenzweig. 2016. Human dendritic cells (DCs) are derived from distinct circulating precursors that are precommitted to become CD1c⁺ or CD141⁺ DCs. *J. Exp. Med.* 213:2861–2870. <https://doi.org/10.1084/jem.20161135>

Camp, L.A., and S.L. Hofmann. 1993. Purification and properties of a palmitoyl-protein thioesterase that cleaves palmitate from H-Ras. *J. Biol. Chem.* 268:22566–22574.

Cebrian, I., G. Visentin, N. Blanchard, M. Jouve, A. Bobard, C. Moita, J. Enninga, L.F. Moita, S. Amigorena, and A. Savina. 2011. Sec22b regulates phagosomal maturation and antigen crosspresentation by dendritic cells. *Cell.* 147:1355–1368. <https://doi.org/10.1016/j.cell.2011.11.021>

Das, A.K., J.J. Bellizzi III, S. Tandel, E. Biehl, J. Clardy, and S.L. Hofmann. 2000. Structural basis for the insensitivity of a serine enzyme (palmitoyl-protein thioesterase) to phenylmethylsulfonyl fluoride. *J. Biol. Chem.* 275:23847–23851. <https://doi.org/10.1074/jbc.M002758200>

Delamarre, L., M. Pack, H. Chang, I. Mellman, and E.S. Trombetta. 2005. Differential lysosomal proteolysis in antigen-presenting cells determines antigen fate. *Science.* 307:1630–1634. <https://doi.org/10.1126/science.1108003>

den Haan, J.M., S.M. Lehar, and M.J. Bevan. 2000. CD8(+) but not CD8(-) dendritic cells cross-prime cytotoxic T cells in vivo. *J. Exp. Med.* 192:1685–1696. <https://doi.org/10.1084/jem.192.12.1685>

Ding, Y., Z. Guo, Y. Liu, X. Li, Q. Zhang, X. Xu, Y. Gu, Y. Zhang, D. Zhao, and X. Cao. 2016. The lectin Siglec-G inhibits dendritic cell cross-presentation by impairing MHC class I-peptide complex formation. *Nat. Immunol.* 17:1167–1175. <https://doi.org/10.1038/ni.3535>

Edelson, B.T., T.R. Bradstreet, K. Hildner, J.A. Carrero, K.E. Frederick, W. Kc, R. Belizaire, T. Aoshi, R.D. Schreiber, M.J. Miller, et al. 2011. CD8 α (+) dendritic cells are an obligate cellular entry point for productive infection by *Listeria monocytogenes*. *Immunity.* 35:236–248. <https://doi.org/10.1016/j.immuni.2011.06.012>

Forrester, M.T., D.T. Hess, J.W. Thompson, R. Hultman, M.A. Moseley, J.S. Stamler, and P.J. Casey. 2011. Site-specific analysis of protein S-acylation by resin-assisted capture. *J. Lipid Res.* 52:393–398. <https://doi.org/10.1194/jlr.D011106>

Fuertes, M.B., A.K. Kacha, J. Kline, S.R. Woo, D.M. Kranz, K.M. Murphy, and T.F. Gajewski. 2011. Host type I IFN signals are required for antitumor CD8⁺ T cell responses through CD8 α + dendritic cells. *J. Exp. Med.* 208:2005–2016. <https://doi.org/10.1084/jem.20101159>

Guilliams, M., F. Ginhoux, C. Jakubzick, S.H. Naik, N. Onai, B.U. Schraml, E. Segura, R. Tussiwand, and S. Yona. 2014. Dendritic cells, monocytes and macrophages: a unified nomenclature based on ontogeny. *Nat. Rev. Immunol.* 14:571–578. <https://doi.org/10.1038/nri3712>

Gupta, P., A.A. Soyombo, A. Atashband, K.E. Wisniewski, J.M. Shelton, P.J.A. Richardson, R.E. Hammer, and S.L. Hofmann. 2001. Disruption of PPT1 or PPT2 causes neuronal ceroid lipofuscinosis in knockout mice. *Proc. Natl. Acad. Sci. USA.* 98:13566–13571. <https://doi.org/10.1073/pnas.251485198>

Hacker, C., R.D. Kirsch, X.S. Ju, T. Hieronymus, T.C. Gust, C. Kuhl, T. Jorgas, S.M. Kurz, S. Rose-John, Y. Yokota, and M. Zenke. 2003. Transcriptional profiling identifies Id2 function in dendritic cell development. *Nat. Immunol.* 4:380–386. <https://doi.org/10.1038/ni903>

- Helft, J., B. Manicassamy, P. Guernonprez, D. Hashimoto, A. Silvin, J. Agudo, B.D. Brown, M. Schmolke, J.C. Miller, M. Leboeuf, et al. 2012. Cross-presenting CD103+ dendritic cells are protected from influenza virus infection. *J. Clin. Invest.* 122:4037–4047. <https://doi.org/10.1172/JCI60659>
- Helft, J., J. Böttcher, P. Chakravarty, S. Zelenay, J. Huotari, B.U. Schraml, D. Goubau, and C. Reis e Sousa. 2015. GM-CSF Mouse Bone Marrow Cultures Comprise a Heterogeneous Population of CD11c(+)MHCI(+) Macrophages and Dendritic Cells. *Immunity.* 42:1197–1211. <https://doi.org/10.1016/j.immuni.2015.05.018>
- Heng, T.S., and M.W. Painter. Immunological Genome Project Consortium. 2008. The Immunological Genome Project: networks of gene expression in immune cells. *Nat. Immunol.* 9:1091–1094. <https://doi.org/10.1038/ni1008-1091>
- Hernldler-Brandstetter, D., H. Ishigame, R. Shinnakasu, V. Plajer, C. Stecher, J. Zhao, M. Lietzenmayer, L. Kroehling, A. Takumi, K. Kometani, et al. 2018. KLRG1+ Effector CD8+ T Cells Lose KLRG1, Differentiate into All Memory T Cell Lineages, and Convey Enhanced Protective Immunity. *Immunity.* 48:716–729.e8. <https://doi.org/10.1016/j.immuni.2018.03.015>
- Hildner, K., B.T. Edelson, W.E. Purtha, M. Diamond, H. Matsushita, M. Kohyama, B. Calderon, B.U. Schraml, E.R. Unanue, M.S. Diamond, et al. 2008. Batf3 deficiency reveals a critical role for CD8alpha+ dendritic cells in cytotoxic T cell immunity. *Science.* 322:1097–1100. <https://doi.org/10.1126/science.1164206>
- Iborra, S., H.M. Izquierdo, M. Martínez-López, N. Blanco-Menéndez, C. Reis e Sousa, and D. Sancho. 2012. The DC receptor DNGR-1 mediates cross-priming of CTLs during vaccinia virus infection in mice. *J. Clin. Invest.* 122:1628–1643. <https://doi.org/10.1172/JCI60660>
- Iborra, S., M. Martínez-López, S.C. Khouili, M. Enamorado, F.J. Cueto, R. Conde-Garrosa, C. Del Fresno, and D. Sancho. 2016. Optimal Generation of Tissue-Resident but Not Circulating Memory T Cells during Viral Infection Requires Crosspriming by DNGR-1+ Dendritic Cells. *Immunity.* 45:847–860. <https://doi.org/10.1016/j.immuni.2016.08.019>
- Jancic, C., A. Savina, C. Wasmeier, T. Tolmachova, J. El-Benna, P.M. Dang, S. Pascolo, M.A. Gougerot-Pocidalgo, G. Raposo, M.C. Seabra, and S. Amigorena. 2007. Rab27a regulates phagosomal pH and NADPH oxidase recruitment to dendritic cell phagosomes. *Nat. Cell Biol.* 9:367–378. <https://doi.org/10.1038/ncb1552>
- Joffre, O.P., E. Segura, A. Savina, and S. Amigorena. 2012. Cross-presentation by dendritic cells. *Nat. Rev. Immunol.* 12:557–569. <https://doi.org/10.1038/nri3254>
- Joshi, N.S., W. Cui, A. Chandele, H.K. Lee, D.R. Urso, J. Hagman, L. Gapin, and S.M. Kaech. 2007. Inflammation directs memory precursor and short-lived effector CD8(+) T cell fates via the graded expression of T-bet transcription factor. *Immunity.* 27:281–295. <https://doi.org/10.1016/j.immuni.2007.07.010>
- Jung, S., D. Unutmaz, P. Wong, G. Sano, K. De los Santos, T. Sparwasser, S. Wu, S. Vuthoori, K. Ko, F. Zavala, et al. 2002. In vivo depletion of CD11c+ dendritic cells abrogates priming of CD8+ T cells by exogenous cell-associated antigens. *Immunity.* 17:211–220. [https://doi.org/10.1016/S1074-7613\(02\)00365-5](https://doi.org/10.1016/S1074-7613(02)00365-5)
- Kaech, S.M., and W. Cui. 2012. Transcriptional control of effector and memory CD8+ T cell differentiation. *Nat. Rev. Immunol.* 12:749–761. <https://doi.org/10.1038/nri3307>
- Kaech, S.M., and E.J. Wherry. 2007. Heterogeneity and cell-fate decisions in effector and memory CD8+ T cell differentiation during viral infection. *Immunity.* 27:393–405. <https://doi.org/10.1016/j.immuni.2007.08.007>
- Kamphorst, A.O., P. Guernonprez, D. Dudziak, and M.C. Nussenzweig. 2010. Route of antigen uptake differentially impacts presentation by dendritic cells and activated monocytes. *J. Immunol.* 185:3426–3435. <https://doi.org/10.4049/jimmunol.1001205>
- Kim, S.J., Z. Zhang, C. Sarkar, P.C. Tsai, Y.C. Lee, L. Dye, and A.B. Mukherjee. 2008. Palmitoyl protein thioesterase-1 deficiency impairs synaptic vesicle recycling at nerve terminals, contributing to neuropathology in humans and mice. *J. Clin. Invest.* 118:3075–3086. <https://doi.org/10.1172/JCI33482>
- Kim, T.S., S.A. Gorski, S. Hahn, K.M. Murphy, and T.J. Braciale. 2014. Distinct dendritic cell subsets dictate the fate decision between effector and memory CD8(+) T cell differentiation by a CD24-dependent mechanism. *Immunity.* 40:400–413. <https://doi.org/10.1016/j.immuni.2014.02.004>
- Kirkling, M.E., U. Cytlak, C.M. Lau, K.L. Lewis, A. Resteu, A. Khodadadi-Jamayran, C.W. Siebel, H. Salmon, M. Merad, A. Tsigirigos, et al. 2018. Notch Signaling Facilitates In Vitro Generation of Cross-Presenting Classical Dendritic Cells. *Cell Reports.* 23:3658–3672.e6. <https://doi.org/10.1016/j.celrep.2018.05.068>
- Komala Sari, T., S.M. Pritchard, C.W. Cunha, G.A. Wudiri, E.I. Laws, H.C. Aguilar, N.S. Taus, and A.V. Nicola. 2013. Contributions of herpes simplex virus 1 envelope proteins to entry by endocytosis. *J. Virol.* 87:13922–13926. <https://doi.org/10.1128/JVI.02500-13>
- Kretzer, N.M., D.J. Theisen, R. Tussiwand, C.G. Briseño, G.E. Grajales-Reyes, X. Wu, V. Durai, J. Albring, P. Bagadia, T.L. Murphy, and K.M. Murphy. 2016. RAB43 facilitates cross-presentation of cell-associated antigens by CD8alpha+ dendritic cells. *J. Exp. Med.* 213:2871–2883. <https://doi.org/10.1084/jem.20160597>
- Lau, C.M., I. Tiniakou, O.A. Perez, M.E. Kirkling, G.S. Yap, H. Hock, and B. Reizis. 2018. Transcription factor ETV6 regulates functional differentiation of cross-presenting classical dendritic cells. *J. Exp. Med.* 215:2265–2278. <https://doi.org/10.1084/jem.20172323>
- Li, Y., Y. Wang, L. Zou, X. Tang, Y. Yang, L. Ma, Q. Jia, Q. Ni, S. Liu, L. Tang, et al. 2016. Analysis of the Rab GTPase Interactome in Dendritic Cells Reveals Anti-microbial Functions of the Rab32 Complex in Bacterial Containment. *Immunity.* 44:422–437. <https://doi.org/10.1016/j.immuni.2016.01.027>
- Lichty, B.D., A.T. Power, D.F. Stojdl, and J.C. Bell. 2004. Vesicular stomatitis virus: re-inventing the bullet. *Trends Mol. Med.* 10:210–216. <https://doi.org/10.1016/j.molmed.2004.03.003>
- Mackay, L.K., A. Rahimpour, J.Z. Ma, N. Collins, A.T. Stock, M.L. Hafon, J. Vega-Ramos, P. Lauzurica, S.N. Mueller, T. Stefanovic, et al. 2013. The developmental pathway for CD103(+)CD8+ tissue-resident memory T cells of skin. *Nat. Immunol.* 14:1294–1301. <https://doi.org/10.1038/ni.2744>
- Manh, T.P., Y. Alexandre, T. Baranek, K. Crozat, and M. Dalod. 2013. Plasmacytoid, conventional, and monocyte-derived dendritic cells undergo a profound and convergent genetic reprogramming during their maturation. *Eur. J. Immunol.* 43:1706–1715. <https://doi.org/10.1002/eji.201243106>
- Mantegazza, A.R., A.L. Zajac, A. Twelvetrees, E.L. Holzbaur, S. Amigorena, and M.S. Marks. 2014. TLR-dependent phagosomal tubulation in dendritic cells promotes phagosomal cross-talk to optimize MHC-II antigen presentation. *Proc. Natl. Acad. Sci. USA.* 111:15508–15513. <https://doi.org/10.1073/pnas.1412998111>
- Mashayekhi, M., M.M. Sandau, I.R. Dunay, E.M. Frickel, A. Khan, R.S. Goldszmid, A. Sher, H.L. Ploegh, T.L. Murphy, L.D. Sibley, and K.M. Murphy. 2011. CD8alpha(+) dendritic cells are the critical source of interleukin-12 that controls acute infection by *Toxoplasma gondii* tachyzoites. *Immunity.* 35:249–259. <https://doi.org/10.1016/j.immuni.2011.08.008>
- Matheoud, D., N. Moradin, A. Bellemare-Pelletier, M.T. Shio, W.J. Hong, M. Olivier, E. Gagnon, M. Desjardins, and A. Descoteaux. 2013. Leishmania evades host immunity by inhibiting antigen cross-presentation through direct cleavage of the SNARE VAMP8. *Cell Host Microbe.* 14:15–25. <https://doi.org/10.1016/j.chom.2013.06.003>
- Meredith, M.M., K. Liu, G. Darrasse-Jeze, A.O. Kamphorst, H.A. Schreiber, P. Guernonprez, J. Idoyaga, C. Cheong, K.H. Yao, R.E. Niec, and M.C. Nussenzweig. 2012a. Expression of the zinc finger transcription factor zDC (Zbtb46, Btbd4) defines the classical dendritic cell lineage. *J. Exp. Med.* 209:1153–1165. <https://doi.org/10.1084/jem.20112675>
- Meredith, M.M., K. Liu, A.O. Kamphorst, J. Idoyaga, A. Yamane, P. Guernonprez, S. Rihm, K.H. Yao, I.T. Silva, T.Y. Oliveira, et al. 2012b. Zinc finger transcription factor zDC is a negative regulator required to prevent activation of classical dendritic cells in the steady state. *J. Exp. Med.* 209:1583–1593. <https://doi.org/10.1084/jem.20121003>
- Milner, J.J., C. Toma, B. Yu, K. Zhang, K. Omilusik, A.T. Phan, D. Wang, A.J. Getzler, T. Nguyen, S. Crotty, et al. 2017. Runx3 programs CD8+ T cell residency in non-lymphoid tissues and tumours. *Nature.* 552:253–257. <https://doi.org/10.1038/nature24993>
- Moore, M.W., F.R. Carbone, and M.J. Bevan. 1988. Introduction of soluble protein into the class I pathway of antigen processing and presentation. *Cell.* 54:777–785. [https://doi.org/10.1016/S0092-8674\(88\)91043-4](https://doi.org/10.1016/S0092-8674(88)91043-4)
- Myou, S., A.R. Leff, S. Myo, E. Boetticher, J. Tong, A.Y. Meliton, J. Liu, N.M. Munoz, and X. Zhu. 2003. Blockade of inflammation and airway hyperresponsiveness in immune-sensitized mice by dominant-negative phosphoinositide 3-kinase-TAT. *J. Exp. Med.* 198:1573–1582. <https://doi.org/10.1084/jem.20030298>
- Nair-Gupta, P., and J.M. Blander. 2013. An updated view of the intracellular mechanisms regulating cross-presentation. *Front. Immunol.* 4:401. <https://doi.org/10.3389/fimmu.2013.00401>
- Ng, C.T., B.M. Sullivan, and M.B. Oldstone. 2011. The role of dendritic cells in viral persistence. *Curr. Opin. Virol.* 1:160–166. <https://doi.org/10.1016/j.coviro.2011.05.006>

- Oberkampf, M., C. Guillerey, J. Mouriès, P. Rosenbaum, C. Fayolle, A. Bobard, A. Savina, E. Ogier-Denis, J. Enninga, S. Amigorena, et al. 2018. Mitochondrial reactive oxygen species regulate the induction of CD8⁺ T cells by plasmacytoid dendritic cells. *Nat. Commun.* 9:2241. <https://doi.org/10.1038/s41467-018-04686-8>
- Poulin, L.F., Y. Reyat, H. Uronen-Hansson, B.U. Schraml, D. Sancho, K.M. Murphy, U.K. Håkansson, L.F. Moita, W.W. Agace, D. Bonnet, and C. Reis e Sousa. 2012. DNGR-1 is a specific and universal marker of mouse and human Batf3-dependent dendritic cells in lymphoid and non-lymphoid tissues. *Blood*. 119:6052–6062. <https://doi.org/10.1182/blood-2012-01-406967>
- Rebecca, V.W., M.C. Nicastrì, N. McLaughlin, C. Fennelly, Q. McAfee, A. Ronghe, M. Nofal, C.Y. Lim, E. Witze, C.I. Chude, et al. 2017. A Unified Approach to Targeting the Lysosome's Degradative and Growth Signaling Roles. *Cancer Discov.* 7:1266–1283. <https://doi.org/10.1158/2159-8290.CD-17-0741>
- Roberts, E.W., M.L. Broz, M. Binnewies, M.B. Headley, A.E. Nelson, D.M. Wolf, T. Kaisho, D. Bogunovic, N. Bhardwaj, and M.F. Krummel. 2016. Critical Role for CD103(+)/CD141(+) Dendritic Cells Bearing CCR7 for Tumor Antigen Trafficking and Priming of T Cell Immunity in Melanoma. *Cancer Cell*. 30:324–336. <https://doi.org/10.1016/j.ccell.2016.06.003>
- Roche, S., and Y. Gaudin. 2002. Characterization of the equilibrium between the native and fusion-inactive conformation of rabies virus glycoprotein indicates that the fusion complex is made of several trimers. *Virology*. 297:128–135. <https://doi.org/10.1006/viro.2002.1429>
- Rock, K.L., and L. Shen. 2005. Cross-presentation: underlying mechanisms and role in immune surveillance. *Immunol. Rev.* 207:166–183. <https://doi.org/10.1111/j.0105-2896.2005.00301.x>
- Salaun, C., J. Greaves, and L.H. Chamberlain. 2010. The intracellular dynamic of protein palmitoylation. *J. Cell Biol.* 191:1229–1238. <https://doi.org/10.1083/jcb.201008160>
- Salmon, H., J. Idoyaga, A. Rahman, M. Leboeuf, R. Remark, S. Jordan, M. Casanova-Acebes, M. Khudoyazarova, J. Agudo, N. Tung, et al. 2016. Expansion and Activation of CD103(+) Dendritic Cell Progenitors at the Tumor Site Enhances Tumor Responses to Therapeutic PD-L1 and BRAF Inhibition. *Immunity*. 44:924–938. <https://doi.org/10.1016/j.immuni.2016.03.012>
- Samie, M., and P. Cresswell. 2015. The transcription factor TFEB acts as a molecular switch that regulates exogenous antigen-presentation pathways. *Nat. Immunol.* 16:729–736. <https://doi.org/10.1038/ni.3196>
- Sancho, D., O.P. Joffre, A.M. Keller, N.C. Rogers, D. Martínez, P. Hernandez-Falcón, I. Rosewell, and C. Reis e Sousa. 2009. Identification of a dendritic cell receptor that couples sensing of necrosis to immunity. *Nature*. 458:899–903. <https://doi.org/10.1038/nature07750>
- Savina, A., C. Jancic, S. Hugues, P. Guermonprez, P. Vargas, I.C. Moura, A.M. Lennon-Duménil, M.C. Seabra, G. Raposo, and S. Amigorena. 2006. NOX2 controls phagosomal pH to regulate antigen processing during crosspresentation by dendritic cells. *Cell*. 126:205–218. <https://doi.org/10.1016/j.cell.2006.05.035>
- Savina, A., A. Peres, I. Cebrian, N. Carmo, C. Moita, N. Hacohen, L.F. Moita, and S. Amigorena. 2009. The small GTPase Rac2 controls phagosomal alkalinization and antigen crosspresentation selectively in CD8(+) dendritic cells. *Immunity*. 30:544–555. <https://doi.org/10.1016/j.immuni.2009.01.013>
- Schwartz, O., V. Maréchal, S. Le Gall, F. Lemonnier, and J.M. Heard. 1996. Endocytosis of major histocompatibility complex class I molecules is induced by the HIV-1 Nef protein. *Nat. Med.* 2:338–342. <https://doi.org/10.1038/nm0396-338>
- Sheridan, B.S., and L. Lefrançois. 2011. Regional and mucosal memory T cells. *Nat. Immunol.* 12:485–491. <https://doi.org/10.1038/ni.2029>
- Sichien, D., C.L. Scott, L. Martens, M. Vanderkerken, S. Van Gassen, M. Plantinga, T. Joeris, S. De Prijck, L. Vanhoutte, M. Vanheerswynghels, et al. 2016. IRF8 Transcription Factor Controls Survival and Function of Terminally Differentiated Conventional and Plasmacytoid Dendritic Cells, Respectively. *Immunity*. 45:626–640. <https://doi.org/10.1016/j.immuni.2016.08.013>
- Sigal, L.J., S. Crotty, R. Andino, and K.L. Rock. 1999. Cytotoxic T-cell immunity to virus-infected non-haematopoietic cells requires presentation of exogenous antigen. *Nature*. 398:77–80. <https://doi.org/10.1038/18038>
- Silvin, A., C.I. Yu, X. Lahaye, F. Imperatore, J.B. Brault, S. Cardinaud, C. Becker, W.H. Kwan, C. Conrad, M. Maurin, et al. 2017. Constitutive resistance to viral infection in human CD141⁺ dendritic cells. *Sci. Immunol.* 2:eaai8071. <https://doi.org/10.1126/sciimmunol.aai8071>
- Sosinowski, T., J.T. White, E.W. Cross, C. Haluszczak, P. Marrack, L. Gapin, and R.M. Kedl. 2013. CD8 α + dendritic cell trans presentation of IL-15 to naive CD8⁺ T cells produces antigen-inexperienced T cells in the periphery with memory phenotype and function. *J. Immunol.* 190:1936–1947. <https://doi.org/10.4049/jimmunol.1203149>
- Spranger, S., D. Dai, B. Horton, and T.F. Gajewski. 2017. Tumor-Residing Batf3 Dendritic Cells Are Required for Effector T Cell Trafficking and Adoptive T Cell Therapy. *Cancer Cell*. 31:711–723.e4. <https://doi.org/10.1016/j.ccell.2017.04.003>
- Stegmann, T., F.P. Booy, and J. Wilschut. 1987. Effects of low pH on influenza virus. Activation and inactivation of the membrane fusion capacity of the hemagglutinin. *J. Biol. Chem.* 262:17744–17749.
- Theisen, D.J., J.T. Davidson IV, C.G. Briseño, M. Gargaro, E.J. Lauron, Q. Wang, P. Desai, V. Durai, P. Bagadia, J.R. Brickner, et al. 2018. WDFY4 is required for cross-presentation in response to viral and tumor antigens. *Science*. 362:694–699. <https://doi.org/10.1126/science.aat5030>
- Tussiwand, R., B. Everts, G.E. Grajales-Reyes, N.M. Kretzer, A. Iwata, J. Bagaitkar, X. Wu, R. Wong, D.A. Anderson, T.L. Murphy, et al. 2015. Klf4 expression in conventional dendritic cells is required for T helper 2 cell responses. *Immunity*. 42:916–928. <https://doi.org/10.1016/j.immuni.2015.04.017>
- Veit, M. 2012. Palmitoylation of virus proteins. *Biol. Cell*. 104:493–515. <https://doi.org/10.1111/boc.201200006>
- Vesa, J., E. Hellsten, L.A. Verkruyze, L.A. Camp, J. Rapola, P. Santavuori, S.L. Hofmann, and L. Peltonen. 1995. Mutations in the palmitoyl protein thioesterase gene causing infantile neuronal ceroid lipofuscinosis. *Nature*. 376:584–587. <https://doi.org/10.1038/376584a0>
- Watts, C. 1997. Capture and processing of exogenous antigens for presentation on MHC molecules. *Annu. Rev. Immunol.* 15:821–850. <https://doi.org/10.1146/annurev.immunol.15.1.821>
- Weed, D.J., S.M. Pritchard, F. Gonzalez, H.C. Aguilar, and A.V. Nicola. 2017. Mildly Acidic pH Triggers an Irreversible Conformational Change in the Fusion Domain of Herpes Simplex Virus 1 Glycoprotein B and Inactivation of Viral Entry. *J. Virol.* 91:e02123-16. <https://doi.org/10.1128/JVI.02123-16>
- Wherry, E.J., and M. Kurachi. 2015. Molecular and cellular insights into T cell exhaustion. *Nat. Rev. Immunol.* 15:486–499. <https://doi.org/10.1038/nri3862>
- Yamazaki, C., M. Sugiyama, T. Ohta, H. Hemmi, E. Hamada, I. Sasaki, Y. Fukuda, T. Yano, M. Nobuoka, T. Hirashima, et al. 2013. Critical roles of a dendritic cell subset expressing a chemokine receptor, XCR1. *J. Immunol.* 190:6071–6082. <https://doi.org/10.4049/jimmunol.1202798>
- Yang, C.Y., J.A. Best, J. Knell, E. Yang, A.D. Sheridan, A.K. Jesionek, H.S. Li, R.R. Rivera, K.C. Lind, L.M. D'Cruz, et al. 2011. The transcriptional regulators Id2 and Id3 control the formation of distinct memory CD8⁺ T cell subsets. *Nat. Immunol.* 12:1221–1229. <https://doi.org/10.1038/ni.2158>